The Lyngen Magmatic Complex ophiolite: preservation of pre- and syn-collisional structures and implications for the nappe thrusting sequence in the Northern Norwegian Caledonides

Marina Galindos-Alfarache, Holger Stünitz, Mathieu Soret, Guillaume Bonnet, Benoît Dubacq, Morgan Ganerød

Tectonophysics 904 (2025) 230706

Contents lists available at ScienceDirect

Tectonophysics

journal homepage: www.elsevier.com/locate/tecto

The Lyngen Magmatic Complex ophiolite: preservation of pre- and *syn*-collisional structures and implications for the nappe thrusting sequence in the Northern Norwegian Caledonides

Marina Galindos-Alfarache [a,*], Holger Stünitz [a,b], Mathieu Soret [b,c], Guillaume Bonnet [d], Benoît Dubacq [e], Morgan Ganerød [f]

[a] Department of Geosciences, UiT-The Arctic University of Norway, Norway
[b] Institut des Sciences de la Terre d'Orléans, University of Orléans, France
[c] Laboratoire de Géologie, UMR 8538, Ecole Normale Supérieure, Université PSL, 75005 Paris, France
[d] Institute of Geological Sciences, University of Bern, Baltzestrasse 1+3, 3012 Bern, Switzerland
[e] Sorbonne Université, CNRS-INSU, Institut des Sciences de la Terre de Paris, ISTeP UMR 7193, F 75005 Paris, France
[f] Norges Geologiske Undersøkelse (NGU), Trondheim, Norway

ARTICLE INFO

Keywords:
North Norwegian Caledonides
Nappe transport sequence
Ophiolite
Geochronology
Raman spectroscopy
Phase equilibrium modelling

ABSTRACT

The Lyngen Magmatic Complex (Northern Norway) marks a major discontinuity in the metamorphic gradient of the North Norwegian Caledonides nappe sequence. The Lyngen Magmatic Complex preserves pre- and *syn*-collisional structures and parageneses of the Caledonian orogeny. This study differentiates the two deformation events and offers a tectono-metamorphic model for the region, using a combination of field-based data, geochemical analysis, radiochronometric dating, and thermodynamic modelling. It is demonstrated that the precollisional event (D1) developed in a dextral strike-slip transpressional regime, generating N—S-trending subvertical shear zones with subhorizontal shear displacement and steeply inclined isoclinal folding. The D1 metamorphic fabrics developed at 486 ± 9 Ma on a retrograde temperature-path, from amphibolite (680—800 °C, 0.5—0.9 GPa) to greenschist facies (300—450 °C, 0.3—0.75 GPa) conditions. The subsequent *syn*-collisional event (D2) produced a subhorizontal foliation, top-to-SE-directed thrust deformation at the base of the Lyngen Magmatic Complex. D2 rock fabrics represent typical nappe stacking structures during the Scandian collisional stage (~430 Ma). The vertical D1 structures are overprinted by D2 fabrics in the thrust contact region only. Mineral assemblages crystallizing during D2 indicate a transition from lower amphibolite to greenschist conditions. Thermobarometry suggests significant re-heating after D1, with D2 maximum conditions ~650 °C and 1.1 GPa at the base of the Lyngen Magmatic Complex and ~558—610 °C and 0.8—1.3 GPa for the underlying graphite-bearing metasediments. Argon dating and the temperature difference between the Lyngen Magmatic Complex and the underlying units testify to out-of-sequence thrusting at 426 ± 7.5 Ma at the base of the Lyngen Magmatic Complex. The present results constrain the localization of the oceanic units of the North Norwegian Caledonides outboard and to the North of their present position. Consequently, stacking of uppermost units (likely of Laurentian origin) on top of the Lyngen Magmatic Complex occurred before their final emplacement onto the Reisa Nappe Complex (probably mostly Baltica-derived).

1. Introduction

Oceanic crust, created at ocean ridges, is consumed in subduction zones (e.g., Wilson, 1965), hence modern oceanic crust records <200 Ma of history of the ocean floor (e.g., Brown, 2009; Agard et al., 2023). During orogenic events, remnants of oceanic lithosphere (i.e., parts of oceanic crust and mantle) can become incorporated within orogenic assemblies (e.g., Dewey, 1976; Searle and Cox, 1999; Wakabayashi and Dilek, 2003) and therefore preserve information otherwise lost. These remnants, defined as ophiolites (e.g., Pearce, 2003), constitute the only accessible rock record of the oceanic lithosphere. Ophiolites allow the reconstruction of long-term evolution of the oceanic lithosphere, from

* Corresponding author.
E-mail address: marina.galindos@uit.no (M. Galindos-Alfarache).

https://doi.org/10.1016/j.tecto.2025.230706
Received 21 August 2024; Received in revised form 5 March 2025; Accepted 8 March 2025
Available online 14 March 2025

birth to demise (e.g., Casey and Dewey, 1984; Dilek and Flower, 2003; Brown et al., 2006; Dilek and Furnes, 2011; among others). Ophiolite preservation is globally scarce and mostly associated to supra-subduction zone settings (e.g., Troodos ophiolite in Cyprus and the Semail Nappe in Oman; Pearce et al., 1984). Metamorphism of ophiolites during orogenesis generally erases the pre-orogenic history of ophiolites (e.g., Rubatto and Angiboust, 2015) but deformation textures and metamorphic assemblages may allow distinguishing pre-orogenic (forearc-back-arc-related) from syn-orogenic tectonic events. Syn-orogenic metamorphism and deformation are often polyphase: gathering petrochronological information such as pressure-temperature-time paths from ophiolites and associated autochthon and allochthon nappes is required to establish the spatial and temporal evolution of the deep orogenic wedge (Soret et al., 2019).

The Norwegian Caledonides include particularly well-preserved ophiolites (e.g., Dunning and Pedersen, 1988; Furnes et al., 1988; Grenne, 1989; Eide and Lardeaux, 2002; Slagstad et al., 2014). The Caledonian orogen is a 6600-km long orogenic belt that results from the continental collision between Baltica and Laurentia in Silurian to Devonian times, with the closure of the Iapetus Ocean (Torsvik et al., 1996; McKerrow et al., 2000; Cocks and Torsvik, 2002). Norway presents several ophiolitic bodies formed between 497 Ma (Leka ophiolite) and 443 Ma (Solund-Stavfjord ophiolite) (Slagstad et al., 2020) after initial rifting of the Iapetus Ocean around 570 to 560 Ma (Roberts et al., 2006).

The Lyngen Magmatic Complex (LMC) is the northernmost and largest ophiolite in Norway (ca. 100 km in length). Its lower mid-ocean crust section exhibits a distinctive supra-subduction zone geochemical signature (Kvassnes et al., 2004) characteristic of forearc-back-arc systems. Corresponding pre-collisional structures are partly overprinted by those generated during the Scandian phase of the Caledonian collision. Consequently, our current understanding of the long-term evolution of the LMC, from seafloor spreading to collision, remains limited, particularly regarding its relations with the surrounding Caledonian nappes and adjacent metasedimentary units like the Eidnas Formation and Balsfjord Group. This study focuses on the tectono-metamorphic history of the LMC and brings new perspectives on the pressure-temperature-time history of the deformation events affecting the ophiolitic body. Field-based structural analysis, geochemical and thermobarometric analysis, phase equilibrium modelling, Raman spectroscopy, U—Pb and $^{40}Ar/^{39}Ar$ geochronology are combined to distinguish between pre- and *syn*-collisional structures. Additional structural, geochemical, thermometric, and thermobarometric data are presented for the Eidnas Formation and Balsfjord Group. New data provided in this study provides a new perspective on the Scandian thrusting sequence and the regional interpretation of the North Norwegian Caledonides. The LMC provides rare information on how strain and fluid-rock interactions localize during the long-term evolution of the oceanic lithosphere in an extensional to convergent settings.

2. Geological setting

The LMC is located in the North Norwegian Caledonides (Fig. 1). Tectonostratigraphically, the LMC is in a key position: located directly below the uppermost units (Corfu et al., 2014), the LMC marks the tectonic and paleogeographic position between units of the Baltica continental margin and/or outer Baltica-related terrains below, and those of Laurentia-related terrains, also referred to as terrains exotic to Baltica above (i.e., Uppermost Allochthon, according to Gee et al., 2014 among others; Fig. 1a). The Northern Scandinavian Caledonides are formed by a sequence of nappes overlying (para)autochthonous metasediments (Dividal Group) covering the Baltica basement (Fig. 1a). Top-to-SE and top-to-E shear senses indicate the transport direction of nappes during Scandian continental collision and W-directed subduction of the Baltica lithosphere (Rice, 1998).

From bottom to top, nappes in the Northern Scandinavian Caledonides are represented by: (1) the Kalak Nappe Complex, with metasedimentary and metaigneous rocks, (2) the Reisa Nappe Complex, which contains metasedimentary and meta-igneous rocks, subdivided into the Nordmannvik, Kåfjord, and Vaddas nappes, (3) the Lyngsfjellet Nappe, divided into the ophiolitic LMC and the overlying metasedimentary Balsfjord Group, (4) the Nakkedal Nappe Complex, with schists, gneisses and migmatites, and (5) the Tromsø Nappe Complex (Uppermost Allochthon), with eclogites, amphibolites, and ultramafics associated to metasedimentary rocks. Units (1) and (2) are Baltica-derived or outboard-Baltica terrains, whereas units (4) and (5) are likely of Laurentian affinity (e.g., Gee and Stephens, 2020; Fassmer et al., 2020) (Fig. 1a). In a different view, unit (5) has been proposed as part of the continental margin of Baltica (Janák et al., 2012). Unit (3) has been part of the oceanic crust of the Iapetus Ocean (e.g., Furnes and Pedersen, 1995). The metamorphic grade within the nappe sequence increases from greenschist in the parautochthonous to upper amphibolite or lower granulite in the Nordmannvik Nappe (unit 2) (Andresen et al., 1985; Bergh and Andresen, 1985; Elvevold, 1988; Lindstrøm and Andresen, 1992). Upwards in the nappe stack, the metamorphic grade sharply decreases to greenschist at the base of the LMC (unit 3) and increases towards the top of the sequence (Andresen et al., 1985; Andresen and Bergh, 1985; Andresen and Steltenpohl, 1994), with amphibolite facies in the Nakkedal Nappe (unit 4) and eclogite metamorphic facies in the Tromsø Nappe Complex (unit 5) (Coker-Dewey et al., 2000; Corfu et al., 2003; Ravna and Roux, 2006; Janák et al., 2012). Therefore, the LMC marks a major discontinuity in the metamorphic gradient of the North Norwegian Caledonides nappe sequence. The nappe sequence is also marked by a structural discontinuity: most nappes are present with low angle foliations developed during Scandian collision (Faber et al., 2019), whereas the LMC displays subvertical structures in large parts of the unit. These two features indicate a distinct evolution of the LMC relative to that of outer-Baltica and Laurentian terrains.

Gravity profiles across the LMC show that the ophiolite has a wedge-shape, dipping towards the west (Chroston, 1972). The latest division of the LMC divides the unit into (1) the Kjosen greenschists, (2) the Lyngen Gabbro, and (3) the Aksla volcanics (Furnes and Pedersen, 1995). The present study retains this classification. For simplicity, the results are framed within the broader term LMC, but distinguishing the metasedimentary Eidnas Formation located between the LMC and the Reisa Nappe Complex (Zwaan et al., 1998; Fig. 1a) and sampled here for thermometric analysis. Some authors included this unit within the Kjosen greenschists (at the base; Oliver and Krogh, 1995) whereas others suggest it as a distinct unit below the LMC but within the Lyngsfjellet Nappe (Zwaan et al., 1998). In any case, the Eidnas Formation is separated from the upper metamorphosed magmatic rocks by a minor thrust, and from the lower Nordmannvik Nappe (unit 2) by a major thrust (Oliver and Krogh, 1995; Zwaan et al., 1998).

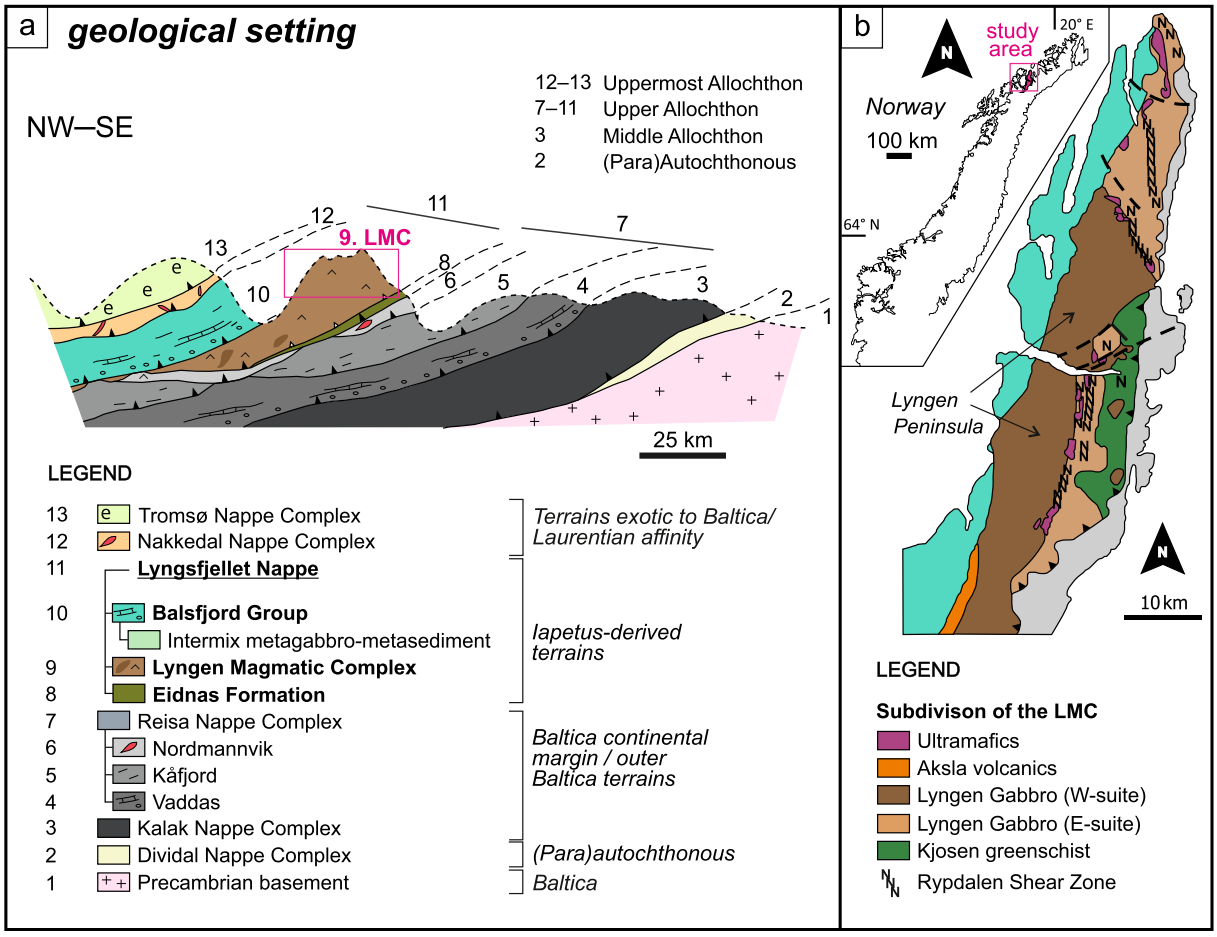

Fig. 1. a) Cross-section of the nappe structures of the Northern Norwegian Caledonides, modified after Augland et al. (2014). The original author exaggerated the cross-section by ca. 3× for clarity. b) Map view of the Lyngen Magmatic Complex, subdivision of units based on the classification from Furnes and Pedersen (1995), modified from Kvassnes et al. (2004).

2.1. The Eidnas Formation

The Eidnas Formation is constituted by westward-dipping graphite-bearing metasediments. This unit has been interpreted as deep-water black shales (Oliver and Krogh, 1995) because of its position in the tectonostratigraphic sequence between the Reisa Nappe Complex (mainly Baltica-derived) and the overlying LMC (Oliver and Krogh, 1995). The metasediments are strongly deformed and metamorphosed, with Grt-bearing mica schists and garnet-free phyllites. Phase equilibrium modelling established a prograde metamorphic evolution from garnet zonation (Schiffer, 2017): pressure-temperature (P-T) conditions range from 515—535 °C and 0.60—0.75 GPa in garnet cores to 580—625 °C and 1.0—1.1 GPa in garnet rims. No ages have been determined for this unit.

2.2. The Lyngen Magmatic Complex

The LMC is subdivided into two magmatic suites on the basis of distinct geochemical signatures (Kvassnes et al., 2004). The Eastern suite (Fig. 1b) is characterized by layered gabbro-norites of boninitic affinity (Furnes and Pedersen, 1995). This suite is intruded by basaltic and tonalitic dykes and tonalitic plutons of various sizes (Furnes and Pedersen, 1995; Selbekk et al., 1998). There are no associated volcanic equivalents. The gabbro-norites crystallized from melts comparable to high-Ca boninitic magmas ultra-depleted in light rare earths from modern forearc settings (Kvassnes et al., 2004). The Western suite (Fig. 1b) is formed by layered gabbros of normal mid-ocean ridge basalt (N-MORB) affinity (Furnes and Pedersen, 1995) and includes basaltic dyke intrusions. Associated volcanics are reported in the upper sections of the ophiolite (i.e., Aksla volcanics; Furnes and Pedersen, 1995; Fig. 1b). The Western suite is considered as originating from a back-arc basin setting (Kvassnes et al., 2004). The geochemistry of the LMC indicates formation in an environment analogous to modern incipient arcs subsequently emplaced as outer-arc highs (Kvassnes et al., 2004). In the southern portion (i.e., from the Kjosen fjord to Nordkjosbotn, Fig. 1b), there are several non-tectonic transitions, suggesting magmatism concurred with deformation (Kvassnes et al., 2004).

The Eastern and Western magmatic suites are locally separated by the Rypdalen Shear Zone (Furnes and Pedersen, 1995; Slagstad, 1995a, 1995b; Fig. 1b). This large-scale, high-temperature ($T > 800$ °C; Slagstad, 1995a, 1995b), ductile shear zone extends discontinuously from north to south of the Lyngen Peninsula with ca. 1 km width (Fig. 1b). The Rypdalen Shear Zone was active during the Ordovician (Oliver and Krogh, 1995) and reflects a transpressional regime (Slagstad, 1995a, 1995b). Two phases of shear were identified, with poorly-preserved early sinistral shear followed by dextral slip movement (Slagstad, 1995a, 1995b). The Rypdalen Shear Zone is also cut by *syn-* to post-tectonic boninitic and tonalitic dykes associated to fore-arc settings, indicating an oceanic origin (Furnes and Pedersen, 1995; Selbekk et al., 1998).

There are two types of tonalitic dykes in the Eastern suite of the LMC and within the Rypdalen Shear Zone (Selbekk et al., 1998). The first type is generated by the fractional crystallization of a boninitic magma, whereas the second type is formed by anatexis of mafic rocks (i.e.,

Eastern suite) in presence of a fluid phase (Selbekk et al., 1998). This fluid was characterized as seawater and interpreted as derived from the subducting slab underlying the LMC. Fluid subsequently channelized along the Rypdalen Shear Zone, promoting the anatexis of boninitic to MORB-type gabbro at $P = 0.5$—0.9 GPa and $T = 680$—800 °C (Selbekk et al., 1998). In addition to the Rypdalen Shear Zone, large scale folding, normal, and reverse faults are found in the ophiolitic body (Randall, 1959; Oliver and Krogh, 1995; Slagstad, 1995a, 1995b). The metamorphic grade of the LMC has been described as greenschist to amphibolite (Oliver and Krogh, 1995; Selbekk et al., 1998), but specific P-T conditions remain poorly constrained. Zircon U—Pb dating from a sheared tonalite layer (Holten tonalite), interpreted as one of the two tonalitic dykes described by Selbekk et al. (1998), determined a minimum age of 481 ± 6 Ma (Augland et al., 2014) for the magmatic crystallization of the LMC. Values of 469 ± 5 Ma yield maximum magmatic crystallization ages (Oliver and Krogh, 1995). No ages for deformation or metamorphism have been established.

2.3. The Balsfjord Group

The Balsfjord Group above the LMC is composed of several layers of metasediments (including phyllites, graphitic-limestones, conglomerates, breccias, dolomites, sandstones and quartzites) with lateral lithofacies variations (Minsaas and Sturt, 1985). The petrology, stratigraphy, and fossil content of the Balsfjord Group testify to continental (e.g., fluviatile deposits; Minsaas and Sturt, 1985) and oceanic affinity (shallow marine environment; Olaussen, 1976; Binns and Matthews, 1981). The contact between LMC and Balsfjord Group was originally described as tectonic (Randall, 1959; Munday, 1974; Binns, 1978; Binns and Matthews, 1981) but later re-interpreted as a stratigraphical unconformity due to the presence of irregular erosion surfaces in the southern portion of the Lyngen Peninsula (Fig. 1b; Minsaas and Sturt, 1985; Andresen and Bergh, 1985). The upper contact with the Nakkedal Nappe Complex (unit 4) is defined by a thrust (Zwaan et al., 1998; Coker-Dewey et al., 2000). The metasediments of the Balsfjord Group are overprinted by polyphase deformation and metamorphism (Minsaas and Sturt, 1985). There is no significant increase in strain towards the upper contact of the Balsfjord Group with the Nakkedal Nappe Complex, but the metamorphic grade increases towards the top of the series (Andresen et al., 1985; Coker-Dewey et al., 2000), with P-T conditions ranging from 450 to 620 °C and 0.3 to 0.9 GPa towards the top (Bergh, 1980; Andresen et al., 1985). Depositional ages for the Balsfjord Group were initially defined as late Ordovician to Silurian by fossil fauna (Olaussen, 1976) and later narrowed to Early Silurian (Llandoverian, 444—433 Ma) by Bjørlykke and Olaussen (1981). $^{40}Ar/^{39}Ar$ on hornblende and muscovite have been used to determine peak metamorphism (432 ± 2 Ma) and subsequent cooling (424 ± 1 Ma to 417 ± 1 Ma) (Dallmeyer and Andresen, 1992; Höpfl et al., 2024). Höpfl et al. (2024) defined four deformation stages within the Balsjord Group: (1) a D0–1, representing an early stage of the burial of the Balsfjord Group and reflecting some incipient metamorphic fabric, (2) a D2 formed during ongoing burial, reflecting peak metamorphism and dated at 429 ± 5 Ma (U—Pb dating on titanites), (3) a D3 interpreted as a local expression of strain incompatibility during D2, and (4) a D4 interpreted as local shortening of the Balsfjord Group against the LMC due to rheological differences between both units.

3. Analytical methods

Twenty-one samples were analyzed (11 metamorphosed gabbronorites from the LMC, 5 metasediments of the Eidnas Formation, and 5 metasediments from the Balsfjord Group). The methodology includes geochemistry, geochronology (U—Pb and $^{40}Ar/^{39}Ar$) and several thermometry (chlorite, Zr-in-titanite, and Raman spectroscopy of carbonaceous material), thermobarometric analyses (based on amphibole-plagioclase pairs and chlorite-phengite multi-equilibrium thermobarometry), and phase equilibrium modelling. A detailed description of the analytical methods is provided in supplementary material. Mineral abbreviations are after Whitney and Evans (2010).

4. Results

This section provides a general summary of the Eidnas Formation, LMC and Balsfjord Group. Table 1 provides detailed information on mineral assemblages, foliation and lineation. Mineral chemistry is available in the supplementary material. Fig. 2a includes the localities mentioned in the text.

4.1. Eidnas Formation

4.1.1. Structural data

Two stages of deformation are distinguished within the study area (including the Eidnas Formation, LMC and Balsfjord Group) (Fig. 2a): a D1 event producing subvertical foliations and subhorizontal lineations (S1-L1; Fig. 2b), later overprinted by a D2 event producing more gently dipping to subhorizontal foliations and WNW-ESE-trending lineations (S2-L2; Fig. 2b).

For the Eidnas Formation, a single event is observed (i.e., D2). Typically, the unit shows gently to moderately dipping foliation (15° to 35°) and the stretching lineation is consistently oriented NW-SE with an average plunge of 28°. However, in the northern Lyngen Peninsula, near the locality of Koppangen (Fig. 1b and 2a), the dip of the S2 foliation planes presents a wider variation (~68° to 26°). In this area, larger dip angles are found near the tectonic contacts, but the stretching lineation plunges an average of 56°. At Rottenvikvatnet (Fig. 2b), quartz σ-clasts and local S-C′ fabrics observed in thin-sections indicate top-to-the-W shear (Fig. 3d2 and 3d3).

In the southern Lyngen Peninsula near the locality of Nordkjosbotn (Fig. 1b and 2a), the Eidnas Formation disappears (Fig. 2a). Slightly further north, the Eidnas Formation records similar S2-foliations and L2-stretching lineations as the southern parts of the LMC (i.e., gently dipping foliations and dominant WNW—ESE L2 stretching lineations; stereoplot sH; Fig. 2b). Garnet porphyroblasts indicate top-to-the-E shear senses (Fig. 3d1 and 3d3).

4.1.2. Petrography (D2 event)

Samples from the Eidnas Formation typically include quartz, white mica, and chlorite. Other phases like biotite, graphite, calcite, Ti-phase, dolomite, garnet, plagioclase, zircon, tourmaline, and pyrite (in decreasing order of abundance) have also been found but inconsistently among samples (Table 1). Every sample presents a mylonitic fabric, with minerals strongly oriented parallel to the lineation/foliation. Chlorite after biotite is the primary retrogression reaction (Fig. 4l). Quartz veins exhibit subgrain rotation (SGR) and grain boundary migration (GBM) microstructures (21M121, 21M123, 21M36, 21M46A; Fig. 4m), calcite (21M121) and plagioclase (21M123) locally show twinning. In rare cases, shear senses are conflicting in some samples. For instance, samples 21M121 and 21M123 show S-C′ fabrics suggesting top-to-the-NW shear sense. However, sample 21M123 also contains garnet porphyroblasts with inclusions that indicate counterclockwise rotation of garnet during growth, i.e., top-to-the-SE shear (Fig. 3d3, microphotograph). Most samples indicate top-to-the-SE or top-to-the-E shear senses. For instance, both garnet sigma-clast shapes (21M36; Fig. 3d1, field image) and deformed amphibole grains indicate top-to-the-E shear senses (20M46A).

Sample 20M46A is used for $^{40}Ar/^{39}Ar$ dating in hornblende, biotite, and phengite and was collected near Rieppevatnet (N69°16′19.5″, E019°46′23.8″; Fig. 2a) at the contact with the LMC. The orientation of the sample corresponds to the D2 event. Sample 20M46A is a mylonitic Grt-Amp-Gr-bearing schist with peak metamorphic assemblage consisting of garnet, biotite, white mica, amphibole, ilmenite, plagioclase, quartz, calcite and dolomite. Retrogressive phases include chlorite.

Table 1
Collection of analyzed samples with their respective coordinates, field orientation, and petrography. Small table with a summary of peak metamorphic assemblages.

		GPS coordinates			Field orientation		Petrography													
Unit	Sample	N (° ' ")	E (° ' ")		Dip dir./Dip	Trend/ Plunge	Cpx	Opx	Pl	Grt	Bt	Amp	Ep	Ttn	Chl	Wm	Qz	Other	Graphite	Microstructures
Balsfjord Group	**21M86A**	69 56 47.8	20 12 42.8	?	221/53	154/27					x			x	x	x	x	Ilm		
	19/79G	69 35 27.1	19 51 05.8	D2	287/46	294/46								x	x	x	x	Cal	x	Cal (twins)
	21M83	69 22 20.6	19 40 47.7	?	245/79	320/54			x	±	x		x	±	x	x	x	Cal, Tur, Py, Ilm		Qz (SGR), Cal (twins)
	21M6	69 09 49.7	19 14 14.7	D2	355/27	301/13				x			x		x	x	x	Ilm, Py		Qz (±SGR)
	21M115	69 15 35.5	18 52 36.4	D2	013/72	287/50			±	x					x	x	x	Ilm, ±Cld		Qz (SGR)
Lyngen Magmatic Complex	**21M44**	69 23 41.6	19 54 37.7		unoriented		x	x	x			±	±					Ilm		Pl (twins)
	20M26A	69 58 30.4	20 16 12.2	D1	283/41	209/14			x		x	x	x	x	x		x	Rt		Qz (SGR, GBM)
	20M39B	69 58 36.1	20 17 00.0	D1	246/50	344/14			x		x	x	x	x	x		x	Ilm		Qz (SGR, GBM)
	20M113A	69 35 18.2	20 07 06.6	D1	285/78	194/36			x			x	x	x	±	±	±	±Ilm		
	21M57B	69 21 12.5	19 42 13.6	D1	286/34	345/24			x			x	x	±	x		x			Qz (SGR)
	20M111	69 14 05.4	19 34 02.7	D2	296/28	280/30			x	x		x	x	x	x		x	Ilm		Qz (SGR, ±GBM), Pl (twins)
	21M101	69 31 18.2	20 07 20.3	D2	226/27	307/25			x			x		x	x		x	Ilm, Zrn		Pl (BLG, twins)
	21M5A	69 09 27.9	19 14 01.2	D2	012/19	265/03			x			x	x	x	x		x	±Rt		Qz (SGR, GBM) Pl (BLG, twins)
	21M26	69 16 12.2	19 39 32.7	D2	302/10	272/12			±			x	x	x			±	Ilm		Pl (twins)
	21M135	69 04 59.2	18 19 55.2	D2	217/51	288/27			x		x	x	x	x	±		x	±Ilm		Qz (SGR)
	21M18	69 09 26.1	19 16 04.4	D2	332/21	280/5			x			x	x	±	x		x			Pl (twins)
Eidnas Formation	**21M121**	69 40 48.3	20 15 36.8	D2	285/26	321/20									x	x	x	Cal, Py	x	Qz (SGR, ±GBM), Cal (twins)
	21M123	69 40 43.4	20 15 56.8	D2	258/68	324/44			x	x	x		±	±	±	x	x	Tur, Ilm, Zrn, Ap	x	Qz (SGR, GBM), Pl (twins)
	20M38	69 36 16.6	20 14 42.6	D2	284/42	260/36									x	x	x		x	Qz (±SGR)
	21M36	69 22 41.8	19 57 19.0	D2	297/26	293/30				x	x		x		x	x	x	Cal, Ilm, Zrn	x	Qz (SGR, GBM)
	20M46A	69 16 19.5	19 46 23.8	D2	004/05	294/05			x	x	x	x			x	x	x	Zrn, Ilm, Cal, Dol	x	Qz (SGR, GBM), plg (twins)

Peak Metamorphic Assemblage										
	Cpx	Opx	Pl	Grt	Bt	Amp	Ti-phase	Ep	Chl	Qz
Magmatic	x	x	x	±						
Amphibolite			x	±	±	x	x			x
Epidote-amphibolite			x			x	x	x		x
Greenschist			x			x	x	x	x	x

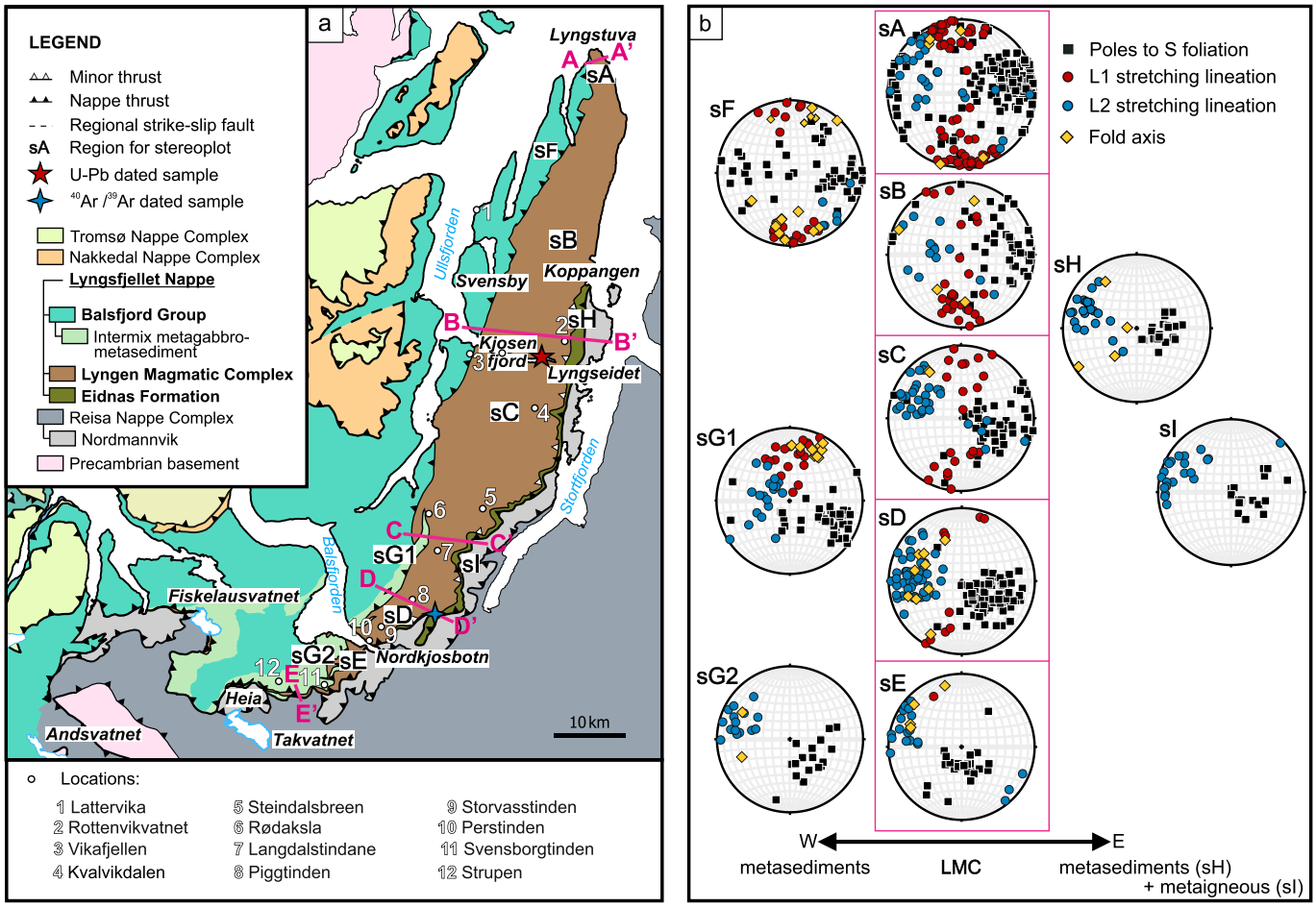

Fig. 2. a) Geological map of the Lyngen Magmatic Complex and surrounding units. Map includes locations mentioned in the main text (numbers), regions for stereoplot projections (small letters), and locations of geochronological samples. b) Stereoplots of field data (lower hemisphere).

Garnet porphyroblasts locally contain ilmenite inclusions, and amphiboles have zircon inclusions. Deformed amphibole grains suggest top-to-the-E shear senses.

Sample 21M123 is used for thermodynamic modelling and was collected near Koppangen (N69°40′43.4″, E020°15′56.8″; Fig. 2a) at the contact between the Eidnas Formation and the Nordmannvik Nappe. The orientation of the sample corresponds to the D2 event (Table 1). Sample 21M123 is a mylonitic Grt-bearing schist that contains garnet, plagioclase, quartz, biotite, white mica, apatite, zircon and ilmenite in the matrix. Minor phases include tourmaline and chlorite. Plagioclase grains show compositional zonation from core to rim (Fig. 4n). Large quartz veins exhibit SGR and minor GBM. The fabric shows S-C′ structures and some Grt- and Pl-porphyroblast show σ-clast shapes. Both indicate top-to-the-NW sense of shear. Grt-porphyroblasts contains quartz, epidote, biotite, apatite, ilmenite, tourmaline, zircon and titanite inclusions (supplementary material). The geometry of the inclusions suggests counterclockwise rotation of garnet during growth (i.e., top-to-the-SE shear). The metamorphic assemblage suggests epidote-amphibolite metamorphic facies.

4.1.3. Mineral chemistry

Plagioclase grains from the Eidnas Formation show albite composition in the core (An_2) and oligoclase composition in the rim (An_{16}) (Fig. 4n and supplementary material).

Garnet crystals show variable zoning patterns, possibly due to non-ideal sections through the crystals. Samples 21M36 and 20M46 present a subtle zonation, whereas it is more developed for sample 21M123. In these samples, garnet cores show a higher content of Mn and Ca compared to the rims (Fig. 5a). For instance, in sample 21M123 the endmembers trend is X_{Alm}(rim/core): 0.60—0.72/0.48—0.62; X_{Grs}(r/c): 0.17—0.26/0.24—0.27, X_{Sps}(r/c): 0.01—0.07/0.06—0.20, and X_{Prp}(r/c): 0.05—0.09/0.03—0.05. The mean grain sizes range from 0.7 mm (21M123) to 2.1 cm in diameter (21M36).

The Eidnas Formation presents higher-grade Grt-bearing micaschists (21M123, 21M36, 20M46A) and lower-grade phyllites (20M38, 21M121). In both cases, chlorite is tri-trioctahedral with 20—40 % amesite and minor sudoite content (Fig. 6a; see Dubacq and Forshaw, 2024 for details). X_{Mg} (=Mg/(Fe^{2+}+Mg)) in higher-grade chlorite ranges over 0.48—0.62 whilst over 2.59—3.36 atoms per formula unit (apfu) for Si. Lower-grade chlorite has X_{Mg} ranging over 0.48—0.58 and Si over 2.62—2.83 apfu (Fig. 6b). White mica corresponds to muscovite with up to 15 % phengitic substitution (Fig. 6d), X_{Mg} values between 0.44 and 0.73 and Si between 3.03 and 3.32 apfu. Most samples of the Eidnas Formation cluster at lower Si-values than the Balsfjord Group, except for sample 20M38 (3.16 to 3.33 apfu) (Fig. 6e).

4.1.4. Geochronology of deformation (D2 event)

Two samples displaying pervasive D2 structures from the southern Lyngen Peninsula were selected for $^{40}Ar/^{39}Ar$ geochronology: (1) a hornblende-bearing metasediment from the Eidnas Formation, close to the lower boundary with the LMC, and (2) a mylonitic retrogressed gabbro-norite at the upper contact with the Balsfjord Group. Yet, only hornblende, biotite, and phengite from sample 20M46A from the Eidnas Formation contained radiogenic Ar to provide results.

Due to the large uncertainty, results for hornblende are not geologically significant and are only included in the supplementary materials.

Table 2
Graphite-bearing and chlorite-bearing metasediments with their respective GPS coordinates. Data includes temperature estimates and standard deviation (SD) for Raman Spectroscopy of Carbonaceous Material (RSCM) and temperature estimates for chlorite based on the thermometer of Vidal et al. (2006).

						Chlorite thermometer (1.1 GPa)		
		GPS coordinates		RSCM		T [°C]		
Unit	Sample	N (° ' ")	E (° ' ")	T [°C]	SD	LT	HT	Average
Balsfjord Group	**20/11**	69 13 43.4	19 11 7.8	519	36			
	20/23	69 30 53.7	19 38 2.2	446	20			
	20/37	69 17 35.9	19 24 52.7	490	33			
	20/77	69 17 38.9	18 59 23.1	510	24			
	21/11	69 25 52.0	19 36 60.0	466	37			
	19/79G	69 35 27.1	19 51 05.8	426	21	329	535	460
	21M6	69 09 49.7	19 14 14.7			357	503	430
	21M83	69 22 20.6	19 40 47.7			345	514	370
	21M85	69 55 40.8	20 11 27.8	447	17			
	21M86A	69 56 47.8	20 12 42.8			310	543	500
	21M87	69 56 37.1	20 12 30.9	499	19			
	21M109	69 15 13.5	19 25 14.0	489	27			
	21M115	69 15 35.5	18 52 36.4			371	474	420
	21M125	69 57 04.6	20 14 01.6	477	25			
	21M127	69 53 59.9	20 06 25.4	491	33			
	21M131	69 46 08.1	19 50 53.6	541	28			
	23M1	69 46 49.0	19 52 49.1	517	21			
	23M5	69 36 33.1	19 47 52.3	442	31			
Lyngen Magmatic Complex	**21M26**	69 16 12.2	19 39 32.7			313	–	310
	21M135	69 04 59.2	18 19 55.2			–	511	510
	21M18	69 09 26.1	19 16 04.4			–	524	525
	21M5A	69 09 27.9	19 14 01.2			325	581	485
	20M38	69 36 16.6	20 14 42.6	507	33	306	–	305
	20M46A	69 16 19.5	19 46 23.8			345	489	445
Eidnas Formation	**20M72**	69 13 59.4	19 34 3.5	559	38			
	21M36	69 22 41.8	19 57 19.0	530	22	304	516	445
	21M48	69 24 02.7	19 01 10.5	534	38			
	21M49	69 24 22.1	19 00 41.6	536	36			
	21M50	69 24 19.1	19 59 55.4	537	30			
	21M121	69 40 48.3	2015 36.8			344	504	425
	21M123	69 40 43.4	20 15 56.8			340	525	490

Fig. 7 presents the $^{40}Ar/^{39}Ar$ analysis results of biotite and phengite. Seventeen heating steps for biotite released ~85 % ^{39}Ar, defining a plateau at 424.51 ± 5.03 Ma (MSDW = 0.73; Fig. 7a). Four heating steps for phengite released ~70 % ^{39}Ar, defining a plateau at 426.61 ± 9.93 Ma (MSDW = 0.46; Fig. 7b). K/Ca ratios reflect large uncertainties, indicating a low ^{37}Ar signal (Fig. 7). The % radiogenic ^{40}Ar shows a plateau in biotite.

4.1.5. Thermobarometry (D2 event)

Phase equilibrium modelling of a Grt-bearing metasediment of the Eidnas Formation, collected close to the lower contact of the Eidnas Formation with the Nordmannvik Nappe (Fig. 2a) (sample 21M123) yield P-T conditions of 550—565 °C and 0.75—0.80 GPa for the garnet core and 600—620 °C and 1.3 GPa for the garnet rim (Fig. 5b and c).

Table 2 presents peak metamorphic temperatures and their standard deviations (SD) obtained by Raman spectroscopy (RSCM, Beyssac et al., 2002) for 6 samples of the Eidnas Formation (lower contact of the LMC) affected by D2 structures. Fig. 8 illustrates the temperature distribution in the area. Samples were taken across strike and with variable proximity to the LMC. Mean temperature values differ somewhat along strike, with ~50 °C variation between samples 20M72 (560 ± 50 °C, near Nordkjosbotn) and 20M38 (510 ± 50 °C, near Koppangen), but the ranges of values overlap. Thus, temperatures may have been slightly higher in the south of the Lyngen Peninsula. There is no significant temperature variation with increasing proximity to the lower boundary of the LMC as shown by samples 21M48, 21M49, and 21M50 (534—537 °C ± 50 °C).

Chlorite-phengite thermobarometry failed to determine equilibrium conditions for co-crystallization of the two minerals. Conversely, crystallization temperatures for chlorite have been estimated following the approach of Vidal et al. (2006, with an approximate error of ± 50°C). Pressure was set at 1.1 GPa as determined by Grt-amphibolite thermobarometry from the LMC for D2. The resulting temperature estimates vary between samples, with a relatively wide spread (e.g., 21M86, 21M83, 21M36; Fig. 6c). Two groups have been identified, one between 300 to ~400 °C (LT) and another between ~400 to ~650 °C (HT; Table 2). The mean crystallization temperature ranges from ~330 to 510 ± 50 °C (~440 ± 50 °C when considered together) for the Eidnas Formation. Results are detailed in the supplementary material.

4.2. Lyngen Magmatic Complex

4.2.1. Structural data

D1 structures are particularly well-preserved in the northern and central regions of the Lyngen Peninsula (Fig. 2b). The LMC foliation planes (S1) range from 50 to 88° dip angle (Fig. 2b, stereoplots sA—sC). The S1 foliation is dipping steeply towards the west. In Lyngstuva, S1 is partially present as magmatic foliation closely associated with a transition to solid-state deformed fabrics. The latter developed under amphibolite and greenschist facies conditions (sub-solidus deformation; Fig. 9a, b, and d). Deformed mafic lenses indicate dextral shear senses (D1: west block-to-the-N; Fig. 3c1). Large-scale tight to isoclinal folds with steeply inclined axial planes (D1 structures; Fig. 2b) are observed in several regions of the northern Lyngen Peninsula, for instance, in Lyngstuva (cross-section A; Fig. 3a and 9c) and the northern coast of the Kjosen fjord (cross-section B; Fig. 3a). Large-scale overturned folds (partially overprinted D1 structures) are observed close to the upper boundary of the LMC (with the Balsfjord Group) on the northern coast of the Kjosen fjord (cross-section B; Fig. 3a). In the northern Lyngen Peninsula, the LMC has a prevalent sub-horizontal, N—S trending stretching lineation (L1; Fig. 2b and 9e).

In the southern Lyngen Peninsula near the locality of Nordkjosbotn

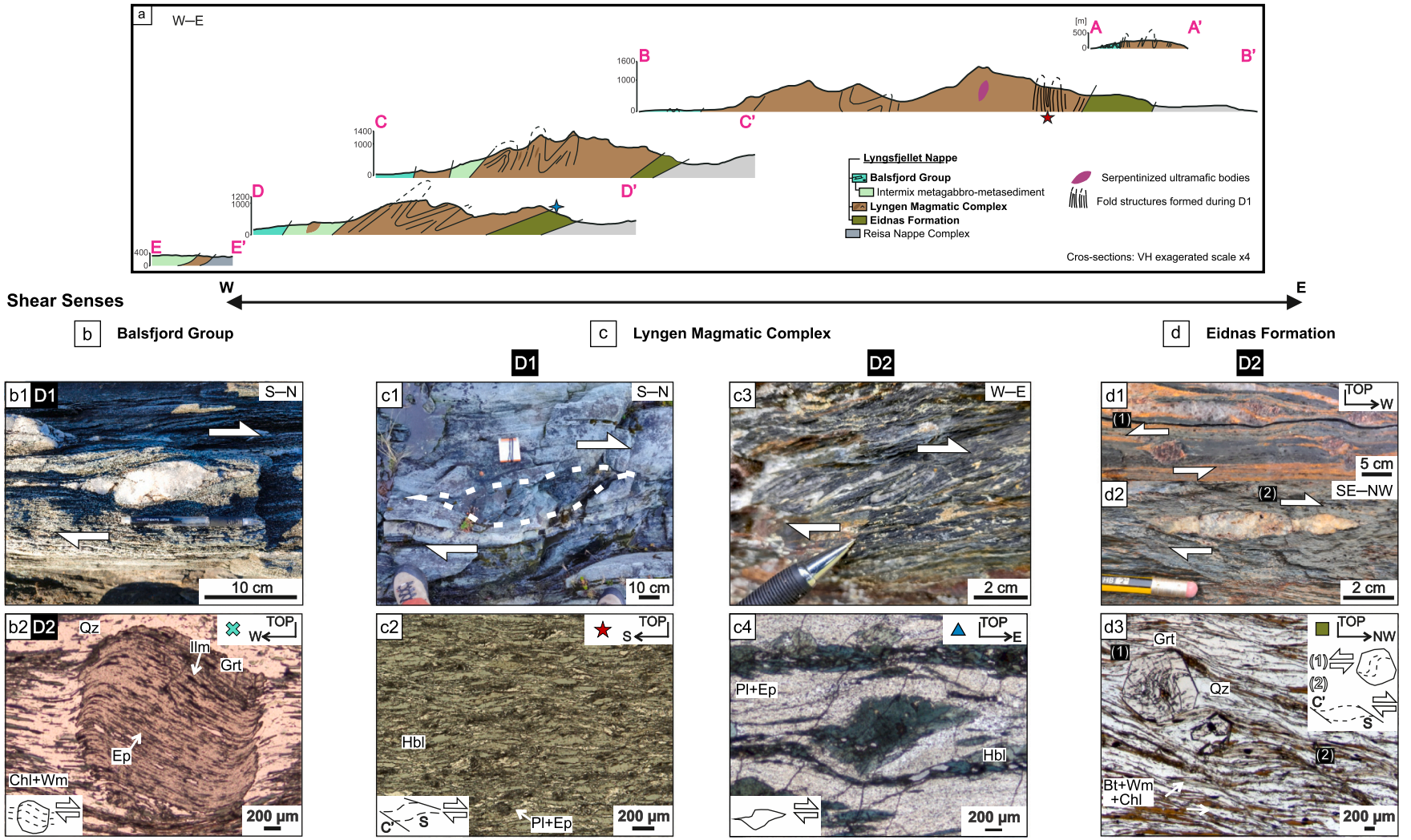

Fig. 3. a) Cross-sections at different locations of the Lyngen Peninsula, locations indicated in map (Fig. 2a). Red five-pointed star indicates location for titanite U—Pb dating, whereas blue four-pointed star indicates location of $^{40}Ar/^{39}Ar$ dating. b to d) Examples of shear sense indicators for both field and thin section. b1) Balsfjord Group: (field) dextrally sheared quartz clast in metasediments adjacent to the Lyngen Magmatic Complex at Lattervika (D1); b2) (Microphotograph) garnet σ-type clast showing top-to-the-E shear sense (D2: sample 21M6). c1) S1-L1 structures of the Lyngen Magmatic Complex: (field) dextrally sheared mafic boudin. Lyngstuva; c2) (Microphotograph) C′-type shear bands indicating top-to-the-N shear sense (D1: 20M113A). c3) S2-L2 structures of the Lyngen Magmatic Complex: (field) sheared folds indicating top-to-the-SE shear sense. Perstinden; c4) (Microphotograph) amphibole σ-type clast showing top-to-the-E shear sense (D2: 21M26). d1) Eidnas Formation: (field) sample of a garnet-bearing metapelite from the same outcrop cut on the XZ plane showing top-to-the-E shear sense. Steindalstinden; d2) Quartz σ-type clast suggesting top-to-the-NW shear sense. Rottenvikvatnet; d3) (Microphotograph) garnet with quartz inclusions indicating anti-clockwise rotation (top-to-the-SE) and C′-type shear bands indicating top-to-the-NW shear sense (D2: sample 21M123). All microphotographs have been captured in plane-polarized light. (For interpretation of the references to colour in this figure legend, the reader is referred to the web version of this article.)

(Fig. 1b and 2a), the LMC becomes much thinner (Fig. 2a). In this region, D2 structures are far better preserved than D1 structures, which D2 obliterated. In the LMC, the foliation planes dip towards the west with varying angles from 84° down to 13° (stereoplots sC—sE; Fig. 2b and 9g). This orientation represents S2 foliations, accompanying deformation overprint and re-orientation of the earlier S1 foliations. Towards Nordkjosbotn, a later WNW—ESE oriented stretching lineation (L2) obliterates the earlier L1. New minerals grow parallel to L2 (e.g., amphibole). In the field, there are top-to-the-SE shear senses for L2 (D2: Fig. 3c3). In some locations, top-to-the-W L2 shear senses are rarely observed in thin section. Local overlap with D1 is present along the Langdalstindane valley (cross-section C) and can be seen in the distance at Svensborgtinden (cross-section E; Fig. 3a and 9h) where gently dipping foliation overprints a steeper foliation. Where the D2 overprint is complete, the LMC is much thinner (cross-sections D and E; Fig. 3a), and all D1 structures (S1 and L1) are obliterated. In the southernmost regions like Storvasstinden, where the thickness of the LMC is strongly reduced, the eastern/ lower contact and foliation of the LMC dips at a lower angle (36° on average) than the western/upper contact (51° on average; Fig. 9i). In the central section, large-scale overturned folds (partially overprinted D1 structures) are observed (e.g., cross-section C; Fig. 3a). Close to Nordkjosbotn, D2 folds have WNW—ESE trending fold axes parallel to the stretching direction, and no D1 structures are preserved.

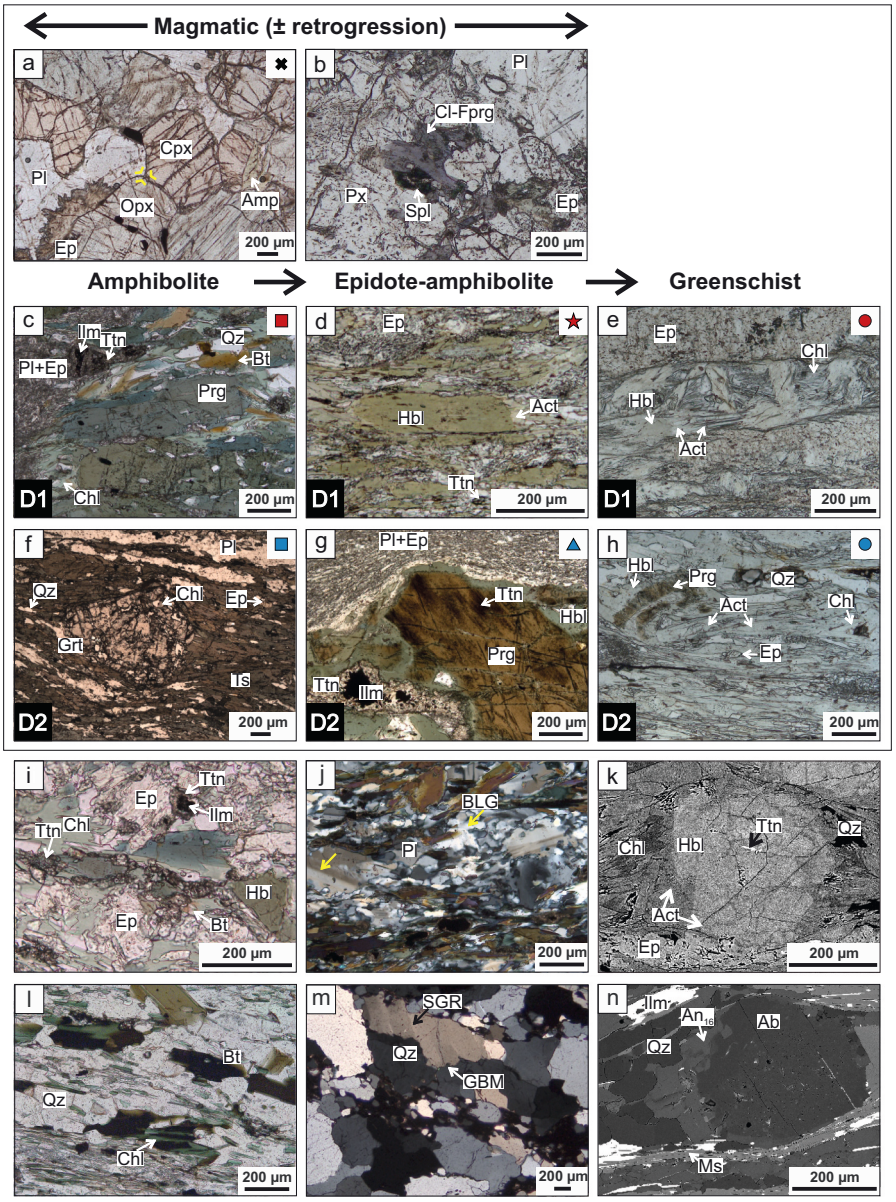

Fig. 4. Thin section microphotographs. a) Undeformed gabbro-norite (sample 21M44). Sample presents a small retrogression visible in the presence of amphibole and epidote. b) Presence of rare chloro-ferro-pargasite, of blue colour (sample 22M24). The sample also shows some retrogression with epidote and spinel. c) Area of the thin section with high-temperature amphibole relict (D1: 20M26A). d) Epidote-amphibolite retrogressed fabric showing amphibole transition from hornblende to actinolite parallel to the stretching lineation (D1: 20M113). e) Greenschist facies fabric (D1: sample 20M57B). f) Garnet-bearing amphibolite sample (D2: 20M111). g) High-temperature, brown-core amphibole (sample 21M26). h) Greenschist facies fabric (D2: 21M18). i) Titanite oriented parallel to the foliation (sample 20M39B). j) Plagioclase exhibiting dynamic recrystallization microstructures (BLG) and twinning (sample 21M101). k) SEM microphotograph of amphibole replacement at greenschist facies (sample 21M57B). l) Chlorite replacement after biotite (sample 21M36). m) High-temperature quartz fabrics (sample 21M36). n) SEM microphotograph plagioclase with albite core and oligoclase rim (sample 20M46). (For interpretation of the references to colour in this figure legend, the reader is referred to the web version of this article.)

4.2.2. Petrography

4.2.2.1. Lyngen Magmatic Complex (magmatic sample). Sample 21M44 is a loose block of meta-gabbro-norite collected at Steindalsbreen (location 5 in Fig. 2a). The fabric is primarily magmatic, with only minor retrogression. The magmatic mineral assemblage includes clinopyroxene, orthopyroxene, and plagioclase (Fig. 4a), locally overprinted by a retrograde assemblage of epidote and amphibole (Fig. 4a). Grain boundaries between magmatic plagioclase, clinopyroxene, and orthopyroxene are hypidiomorphic and show grain interlocking, indicating magmatic contacts between the three phases (Fig. 4a). In addition, locally in Lyngstuva, in situ S1-L1 retrogressed magmatic rocks (sample 22M24) show blue-coloured amphibole (Fig. 4b).

4.2.2.2. Lyngen Magmatic Complex (D1 and D2 events). Magmatic rocks of the LMC were metamorphosed during the two deformation events, D1 and D2. The parageneses described below are based on orientation along D1 and D2. The resulting metamorphic rocks show gradual mineralogical changes that can be ascribed to amphibolite, epidote-amphibolite, and greenschist facies assemblages. Samples range from meta-gabbro-norites up to mylonitic amphibolites or greenschists.

For amphibolite facies (D1: 20M39B, 20M26A; D2: 20M111, 21M101), mineral assemblages typically include green-blue amphibole, plagioclase, quartz, and a Ti-phase (rutile or ilmenite). Locally, biotite (D1: 20M26A) and garnet (D2: 20M111) are found. Most minerals have their long axes oriented parallel to the lineation (Fig. 4c, f, and i). The main difference between D1 and D2 samples is the presence of garnet (D2: 20M111) (Fig. 4f) restricted to the D2 fabrics at the base of the LMC (e.g., Perstinden). SGR and GBM in quartz veins parallel to the foliation (D1: 20M39B, 20M26A; D2: 20M111) have been observed in addition to bulging microstructures (BLMC) in plagioclase (D2: 21M101) (Fig. 4j). In this sample (D2: 21M101), plagioclase is unaltered, largely twinned, partly oriented parallel to the foliation, and shows core-and-mantle-structures.

For epidote-amphibolite facies (D1: 20M113; D2: 21M5A, 21M26, 21M135), mineral assemblages typically include amphibole, plagioclase, quartz, a Ti-phase (titanite), and epidote. Titanite coronas around ilmenite are frequently observed (D2: 21M26, Fig. 4g). The newly crystallizing amphibole is predominantly green (D1: 20M113, Fig. 4d). Brown cores are often preserved in D2 samples (21M26, 21M135; Fig. 4g). Epidote is closely associated with plagioclase. At this metamorphic grade, the matrix minerals (e.g., amphibole, titanite, and epidote) are strongly oriented parallel to the lineation (D1:20M113, D2: 21M5A, 21M26, 21M135; Fig. 4d, g, 11a). In some cases, C′-type shear bands are developed (D1: 20M113; D2: 21M5A). For D1 samples, shear bands indicate west block-to-the-N shear sense (D1; Fig. 3c2) and top-to-the-E for D2. Amphibole (21M26) and plagioclase (21M5A) sigma clasts also indicate top-to-the-E shear for D2 (Fig. 3c4). Quartz veins with SGR and GBM microstructures and twinned plagioclase are locally present (21M5A).

For greenschist facies (D1: 21M57B; D2: 21M18), mineral assemblages typically include amphibole, plagioclase, quartz, a Ti-phase (titanite), epidote, and chlorite. Colourless amphibole and chlorite are abundant. These minerals, and titanite coronas around ilmenite, also locally appear as replacement products in samples of higher metamorphic grade (D1: 20M26A, 20M39B, 20M113; Fig. 4c and i). In the greenschist-facies samples, local amphibole grains are compositionally zoned, showing green (D1: 21M57B; D2: 21M18; Fig. 4e and h), brown (D2: 21M18; Fig. 4h), and colourless amphibole. In these cases, colourless amphibole is not restricted to the tip of the grains (D1: 20M113; Fig. 4d) but is also found in between cleavage planes (D1: 21M57B; D2: 21M18; Fig. 4k). Minerals are strongly oriented parallel to the foliation. In some cases, shear senses are conflicting (D2: 21M18), indicating both top-to-the-W and top-to-the-E shear.

Sample 20M113 is used for U—Pb dating of titanite and was collected next to road 91 between Svensby and Lyngseidet (N69°35′18.4″, E020°07′03.6″; Fig. 2a). The orientation of the sample corresponds to D1 event (Fig. 9e). Under the microscope, elongated titanite grains show a strong shape preferred orientation (SPO) parallel to the foliation plane (Fig. 11a). Grain sizes range between 320 and 610 μm along the longest axis. Smaller grains are found following the same orientation, with sizes up to 20 μm, too small to yield usable U—Pb geochronological results. Titanite contains inclusions of ilmenite and plagioclase, aligned parallel to the foliation plane (Fig. 11b). The peak metamorphic assemblage including titanite indicates epidote-amphibolite P-T-conditions with minor retrogression to greenschist facies.

Sample 20M111 is a Grt-bearing mylonitic amphibolite used for thermobarometry and was collected in Perstinden (N69°14′05.4″, E019°34′02.7″; Fig. 2a). The orientation of the sample corresponds to the D2 event. Under the microscope, the peak metamorphic assemblage consists of garnet, amphibole, plagioclase, ilmenite, and quartz. Epidote after plagioclase and chlorite after garnet indicates minor retrogression of the sample. The amphibole grains are strongly oriented parallel to the foliation plane. Garnet crystals have a small grain size (~0.9 mm), present a very weak compositional zonation (Fig. 5a), and are partly replaced by chlorite. Garnet includes amphibole, titanite, epidote, and quartz, some of which are partly oriented parallel to the lineation, suggesting *syn*-tectonic growth of the garnet.

4.2.3. Mineral chemistry

4.2.3.1. Magmatic sample. The magmatic mineral assemblage (sample 21M44) includes augite, enstatite, and plagioclase (An_{93}) (black crosses in Fig. 10a and b), locally overprinted by a retrograde assemblage made of epidote and Mg-hornblende (black crosses in Fig. 10c). The blue-coloured amphibole of the retrogressed magmatic sample 22M24 in Lyngstuva is composed of Cl-rich ferro-pargasite (ca. 4 wt.% Cl; sample 22M24; supplementary material).

4.2.3.2. Lyngen Magmatic Complex (D1 and D2 events). In samples from the LMC, amphibole composition (based on 23 oxygens; Leake et al., 1997) reveals a decreasing trend for $(Na + K)^A$ and Ti with respect to Si-content (Fig. 10c1 and 10c3) and increasing trend for X_{Mg} vs Si (Fig. 10c2) for both D1 (red symbols) and D2 samples (blue symbols). Samples have been classified into amphibolite (squares), epidote-amphibolite (D1: stars, D2: triangles, diamonds) and greenschist (filled circles) facies based on peak metamorphic mineralogy. Black crosses represent green amphibole derived from the retrogression of pyroxene from the magmatic rock and are used as a reference. Most D1 and D2 amphibole compositions are richer in Mg than Fe (Fig. 10c2) and vary from green-blue/brown pargasite to colourless actinolite (Fig. 10c1). However, amphiboles associated with S2-L2 show a broader spread in the tschermakitic field (Fig. 10c1 and 10c2) than amphiboles associated with S1-L1. In addition, several samples show varying compositions within a single microstructure, reflecting porphyroblasts with core and rim structures. Compositional variations along the grain developed during deformation, evidenced by the geometry of the deformed grain and the compositional variation occurring parallel to the stretching lineation. For instance, sample 20M113 (D1) presents green Mg-hornblende amphibole porphyroblasts with colourless actinolite at the tips of the deformed grain (Fig. 4d). Samples 21M26 and 21M135 (D2) show brown pargasite cores with titanite exsolutions associated with green Mg-hornblende rims in thin-section (Fig. 4g). Samples associated with D2 frequently preserve brown amphibole cores (of pargasitic composition) compared to D1 samples (green amphibole of Mg-hornblende composition). The titanium content in D1 amphibole ranges between <0.01 and 0.11 apfu. (Fig. 10c3). Sample 20M26A (D1) presents high-temperature amphibole relicts with Ti content similar to retrogressed amphibole in magmatic rocks (0.01 to 0.13 apfu). In D2

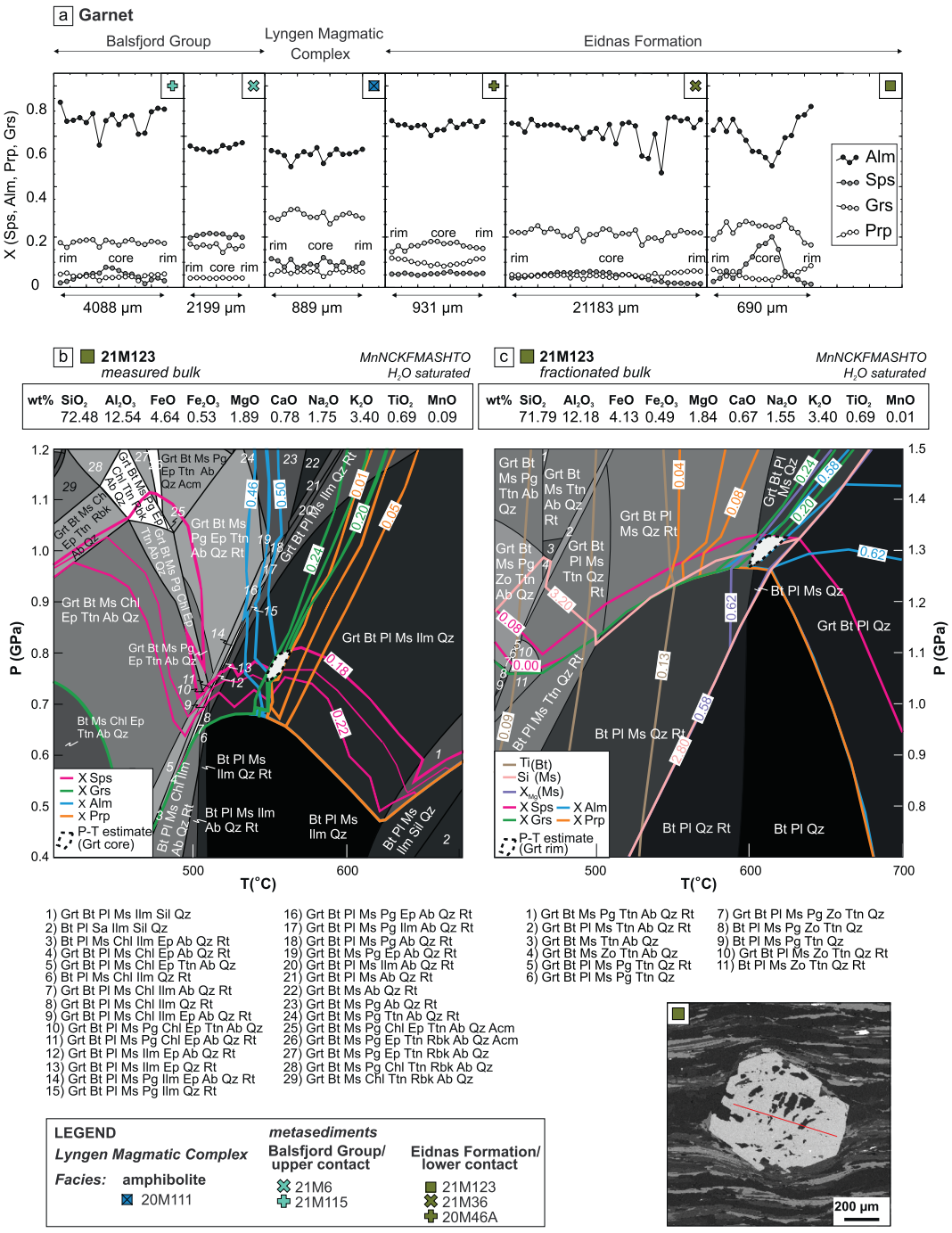

Fig. 5. a) Garnet profiles from rim to rim. Garnets from metasedimentary samples show variable degrees of zonation, except for sample 21M6. Sample from the Lyngen Magmatic Complex (20M111) presents a very weak zonation. b) Pseudo-section calculated with bulk rock composition that reflects garnet core conditions for sample 21M123 (Eidnas Formation). c) Pseudo-section calculated with the fractionated bulk composition that reflects garnet rim conditions for sample 21M123 (Eidnas Formation).

amphibole, values range from <0.01 to 0.13 apfu and outliers points range between 0.13 and 0.27 apfu (Fig. 10c3). These outlier values come from D2 samples 21M18 and 21M26, which present pargasitic cores with titanite exsolutions. The values for the rest of the elements of these point analyses are consistent with amphibole crystal chemistry, precluding possible errors due to contamination.

Plagioclase compositions from the LMC fall mainly in the albite field ($An_{0–10}$; Fig. 10b) for D1 (20M26A, 20M39B, 20M113, 21M57B) and D2 samples (21M101, 21M5, 21M26). S2-L2 fabrics preserve higher-grade plagioclase in the matrix (e.g., from An_{29} to An_0, 20M111; Fig. 10b) compared to S1-L1, which only presents local oligoclase inclusions in Mg-hornblende (20M113).

Samples from the LMC locally contain weakly zoned garnet (D2: 20M111, Fig. 5a). Grains sizes are small (~0.9 mm diameter), and garnet is enriched in the Fe and Ca endmembers (X_{Alm}: 0.48—0.55; X_{Grs}: 0.25—0.31; X_{Sps}: 0.08—0.12; X_{Prp}: 0.04—0.07; see also supplementary materials).

Chlorite composition falls within the daphnite and clinochlore domain with 20—40 % amesite and minor sudoite content (Fig. 6a). Crystals from samples of the LMC present higher X_{Mg} values (0.41—0.73) than those from the adjacent metasedimentary units, consistent with the metabasic nature of the rocks. For samples of the

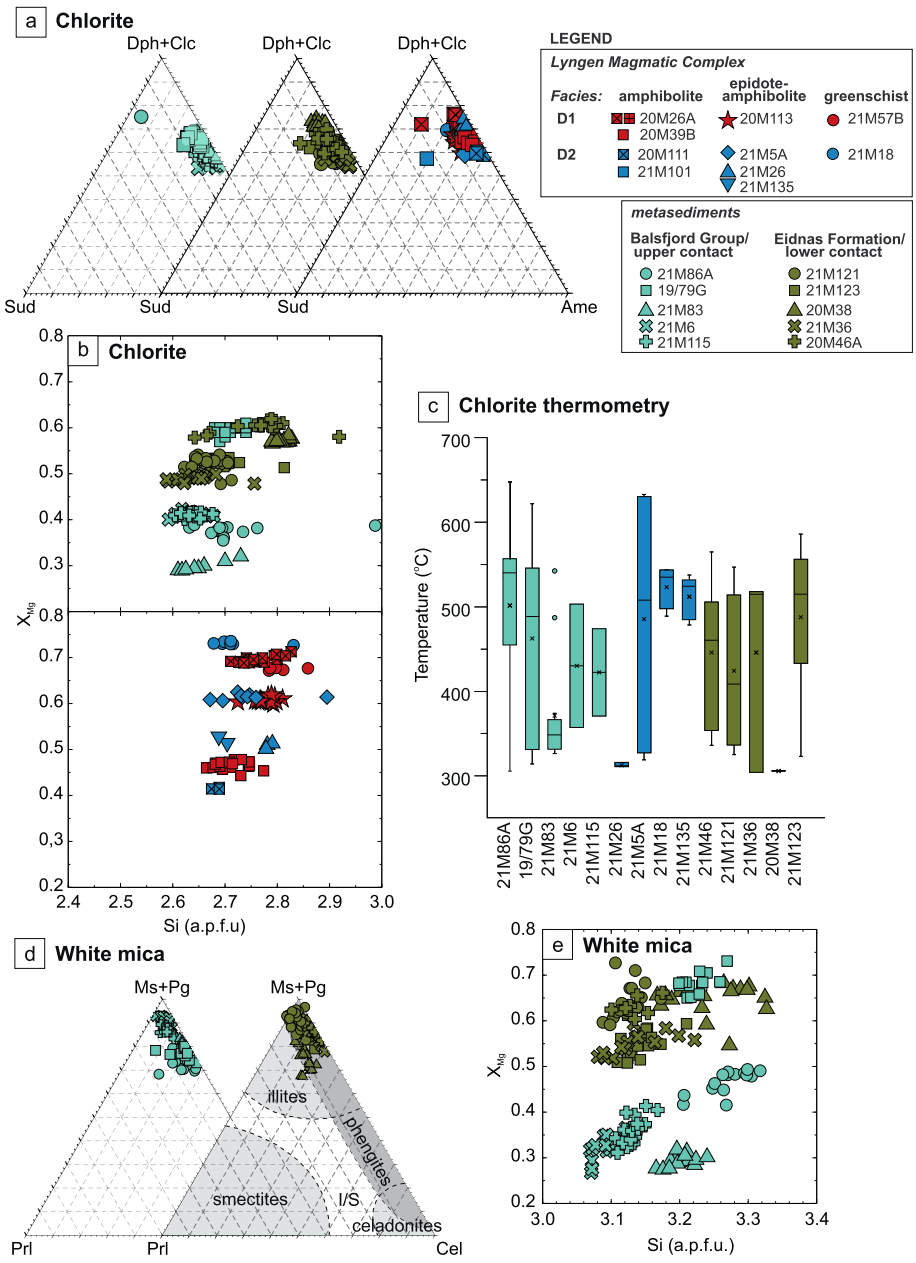

Fig. 6. a) From left to right, chlorite classification for samples from the Balsfjord Group, Eidnas Formation and Lyngen Magmatic Complex. All samples fall within the daphnite and clinochlore domain with 20—40 % amesite and minor sudoite content. b) X_{Mg} v. Si diagrams for chlorite. Samples from the Lyngen Magmatic Complex show higher X_{Mg} values for greenschist facies and lower for amphibolite facies for both S1-L1 and S2-L2. c) Box diagram reflecting chlorite crystallization temperature distribution for the analyzed samples. Vertical lines go from the extremes to the box, which is delimited by the 1st (lower) and 3rd (upper) quartile. Symbols represent average (cross), median (horizontal line), and outliers (circles). d) From left to right, chlorite classification for samples from the Balsfjord Group and Eidnas Formation. All samples fall within the muscovite field with phengitic substitution restricted to a maximum 15 %. e) X_{Mg} v. Si diagrams for white mica. Overall, samples from the Eidnas Formation contain higher X_{Mg} ratios than the Balsfjord Group.

LMC (D1 and D2), X_{Mg} values appear to increase with decreasing metamorphic grade. This trend is also observed in amphibole (Fig. 10c2). Thus, metabasitic samples reflect opposite metamorphic grade—X_{Mg} relation compared to metapelitic rocks. The only exception is D1 sample 20M26A (amphibolite facies; Fig. 6b), which composition falls in the same range as D1 sample 21M57B (greenschist facies). The mismatching results of sample 20M26A might reflect a more pervasive retrogression of the sample compared to the other amphibolite sample for this set (20M39B).

4.2.4. Geochronology of deformation (D1 event)

Titanite and rutile from four samples of the LMC were analyzed. In three samples, low U—Pb and/or low U concentrations (<1 ppm) resulted in low-precision results (included as supplementary material).

The analysis of 37 spots in titanite in the D1 sample 20M113 yielded $^{207}Pb/^{206}Pb$—$^{238}U/^{206}Pb$ discordia age of 485.8 ± 9.3 Ma (2σ, MSWD = 0.8; Fig. 11c). Chondrite-normalized REE patterns indicate two populations, a predominant one showing a positive Eu anomaly and a second one without an Eu anomaly – yet with no significant difference in age (Fig. 11d). Fe/Al ratios plot near or below the 1:2 trend (Fig. 11e), and Zr-in-titanite concentrations average 225 ppm.

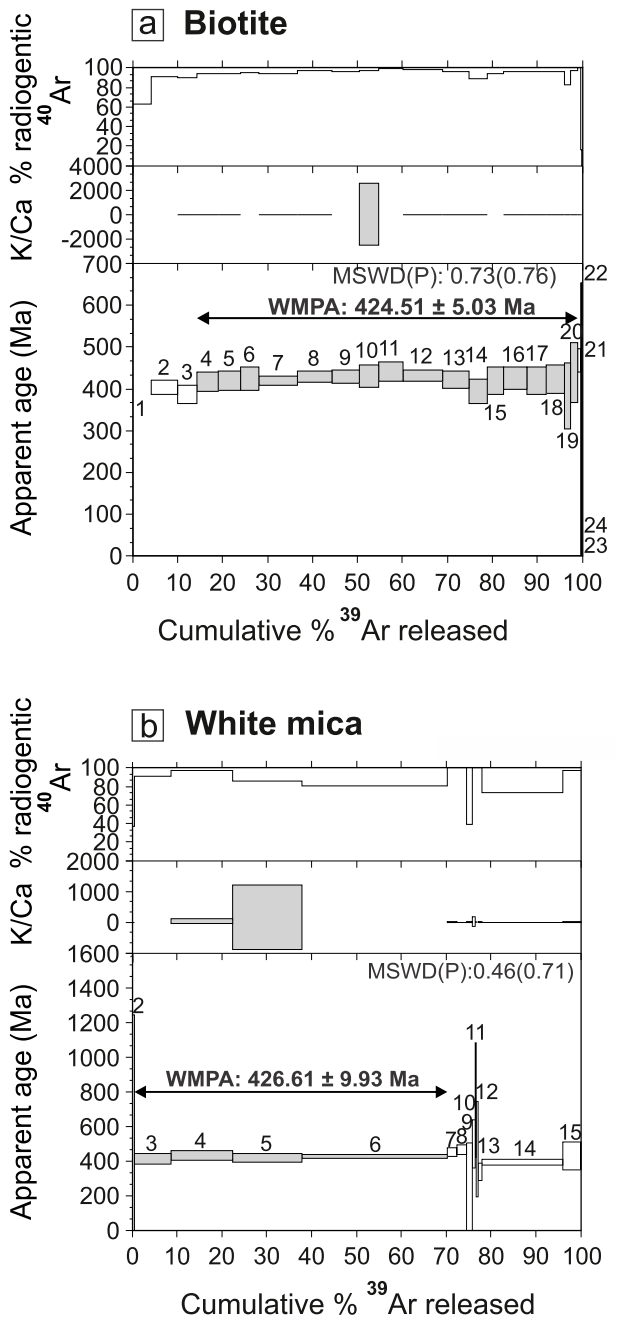

Fig. 7. $^{40}Ar/^{39}Ar$ spectra. Biotite and white mica results represent cooling ages.

4.2.5. *Thermobarometry*

4.2.5.1. D1 event. The thermometer of Holland and Blundy (1994) and the geobarometer of Molina et al. (2015) for plagioclase-amphibole pairs along albite ($An_{0.08}$) and edenite vectors yield average P-T conditions of 650 ± 40 °C and 0.9 ± 0.15 GPa for sample 20M113 (retrogressed gabbro-norite, LMC). The Zr-in-titanite thermometry (Hayden et al., 2008) was used to estimate the temperature in sample 20M113, assuming $a(SiO_2)$ of 1 (confirmed by the presence of quartz in the rock) and $a(TiO_2)$ of 0.75—0.85 (assumed in absence of rutile and presence of ilmenite inclusions; as in Kohn, 2017). Results yield conditions between ~690 ± 20 °C at 0.3 GPa (typical pressure values for ocean floor conditions) and ~760 ± 20 °C at 0.90 GPa (i.e., pressure conditions as those established by conventional Pl-Amp-thermobarometry).

4.2.5.2. D2 event. Plagioclase-amphibole pairs of oligoclase ($An_{0.18}$) and hornblende compositions yield P-T conditions of 650 ± 40 °C and 1.10 ± 0.15 GPa for a Grt-bearing amphibolite (20M111) collected close to the lower contact of the LMC (Fig. 2a and 9c). In addition, the geobarometer of Kohn and Spear (1990) yields an average pressure of 1.10 ± 0.05 GPa at 660 °C. Chlorite thermometry of the samples of the LMC yields a mean crystallization temperature of ~320 to 540 ± 50 °C, averaging ~475 ± 50 °C (supplementary material).

4.3. *Balsfjord Group*

4.3.1. *Structural data*

The Balsfjord Group in contact with the LMC occurs with steeply dipping (towards the west) to vertical S1 foliation and sub-horizontal N—S trending L1-stretching lineation. Deformed quartz clasts indicate dextral shear senses (D1: west block-to-the-N; Fig. 3b1). In the region near Lyngstuva, the Balsfjord Group presents a well-developed cleavage associated with folds with a steeply inclined axial plane to the WNW and gently plunging fold axis (F1: fold axis = 019/17; axial plane = 296/66). Locally, an earlier intrafolial folding phase can be observed transposing the foliation (S0). This earlier F0 is characterized by moderately inclined axial planes to the NNE and gently plunging fold axis (e.g., fold axis = 337/22; axial plane e.g. = 036/38) (Fig. 9f).

At the western boundary of the LMC, the Balsfjord Group has the same orientation as the LMC in the southern section of the Lyngen Peninsula, showing both L1 and L2 close to the contact with the LMC (stereoplot sG; Fig. 2b).

4.3.2. *Petrography (D1 and D2 events)*

Samples from the Balsfjord Group typically include white mica, quartz and chlorite. Additional phases like calcite, Ti-phase, garnet, epidote, graphite, biotite, tourmaline, and chloritoid (in decreasing order of abundance) have been found (not in all samples, Table 1). Every sample presents mylonitic fabrics. Minerals are strongly oriented parallel to the lineation, except for sample 21M86A, which also presents some randomly oriented phases (biotite). Retrograde phases consist of epidote and chlorite after biotite (21M86A) or garnet (21M6, 21M115). Locally, quartz shows SGR microstructures (21M83, 21M115), and calcite is twinned (19/79G). Only two samples indicate shear senses. Sample 21M6 presents *syn*-tectonic garnet with ilmenite, epidote, and quartz inclusions. Top-to-the-E shear senses are derived from the orientation of garnet and ilmenite inclusion trails (Fig. 3b2). Similarly, sample 21M115 presents syn-tectonic garnet with ilmenite and chloritoid inclusions. Shear senses derived from the orientation of inclusion trails suggest top-to-the-E shear.

Finally, between Rødaksla and Strupen (Fig. 2a), there is a mylonitic greenschist subunit within the Balsfjord Group (subunit 48 from Zwaan et al., 1998; light green in Fig. 2a) where it is difficult to identify the protolith of the rocks. The presence of epidote clasts (Fig. 9j) and the transition from meta-gabbro norite to greenschist mylonites (Fig. 9k1 to 9k3) in the subunit, close to the boundary with the LMC, suggest that some of the mylonitic greenschists are derived from retrogressed gabbro of the LMC. Some degree of mixing between lithologies from both units (Balsfjord Group and LMC) is inferred, too, both deformed at low metamorphic grade. The location of the mylonitic greenschist subunit coincides with the beginning of the progressive thinning of the LMC towards the south.

4.3.3. *Mineral chemistry*

In the Balsfjord Group, garnet from sample 21M115 is zoned, whereas those from sample 21M6 are homogenous. Zoning in 21M115 shows spessartine-rich cores (X_{Sps}(r/c): 0.01—0.04/0.04—0.08) and enrichment in almandine and pyrope towards the rim (X_{Alm}(r/c): 0.61—0.73/0.57—0.69; X_{Prp}(r/c): 0.04—0.06/0.03—0.04) (Fig. 5a). The mean grain sizes vary between samples from 0.41 to 0.22 mm in diameter, with larger grains showing greater zoning. The difference

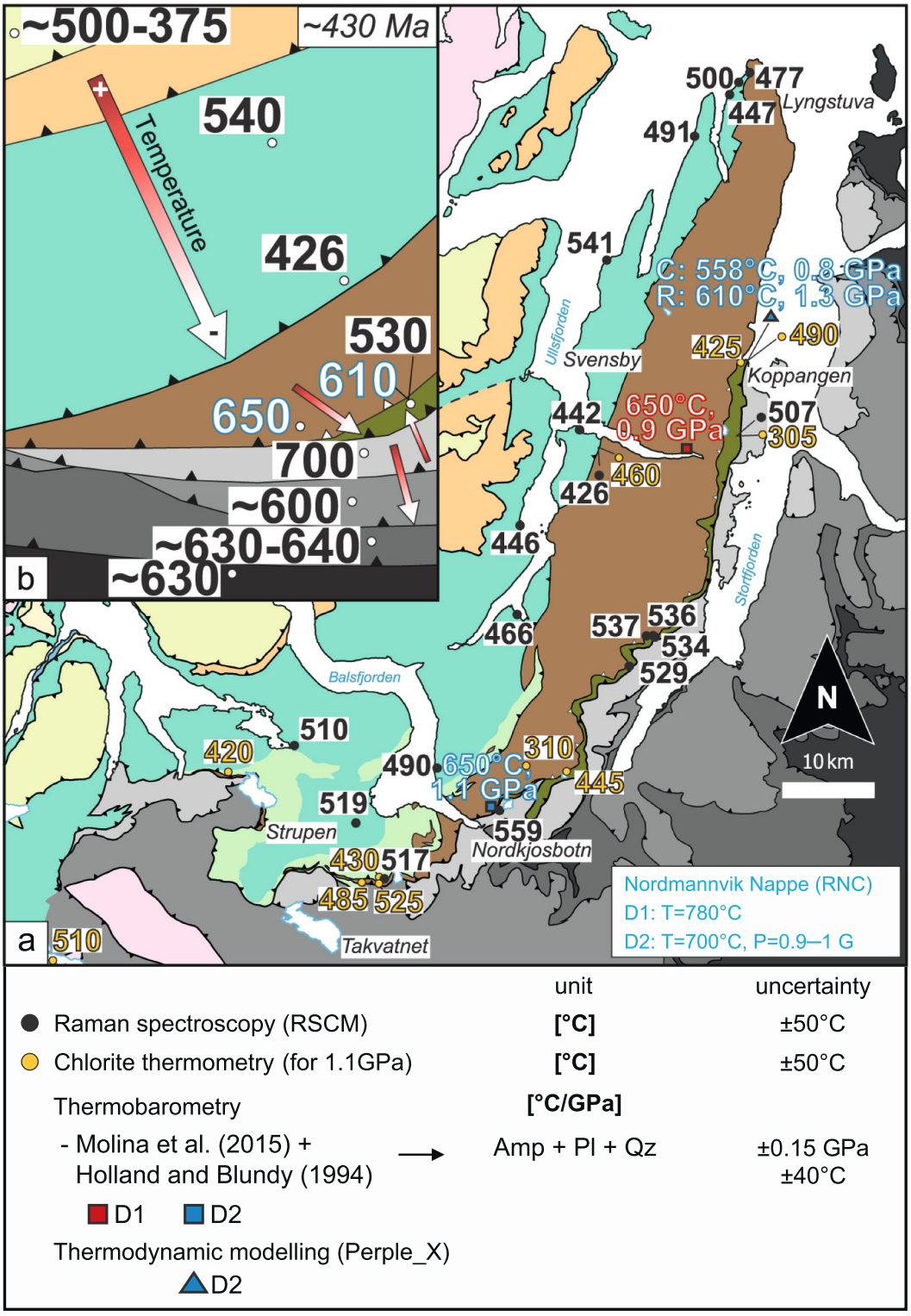

Fig. 8. a) Pressure-temperature distribution for the Lyngen Magmatic Complex and adjacent metasedimentary units. Four methods were used: RSCM, marked with black dots (numbers indicate temperature); chlorite thermometry (for 1.1 GPa), marked with yellow dots (numbers indicate temperature); amphibole-plagioclase geothermobarometry (Lyngen Magmatic Complex, D1: 20M113, small red square; and D2: 20M111, small blue square), and thermodynamic modelling (Eidnas Formation, sample 21M123, blue triangle). b) Sketch illustrating the temperature transition from the upper Tromsø Nappe Complex down to the Kalak Nappe. Temperatures from the Tromsø Nappe, Reisa Nappe Complex, and Kalak Nappe are taken from Krogh et al. (1990), Dallmeyer and Andresen (1992), Faber et al. (2019) and Yogi et al. (2024). Temperatures from the Balsfjord Group, Lyngen Magmatic Complex and Eidnas Formation from this study. Values from this study in black are from RSCM and blue values are from thermobarometric calculations/modelling. Temperature distribution suggests the presence of an out-of-sequence thrust at the base of the Lyngen Magmatic Complex and Eidnas Formation. (For interpretation of the references to colour in this figure legend, the reader is referred to the web version of this article.)

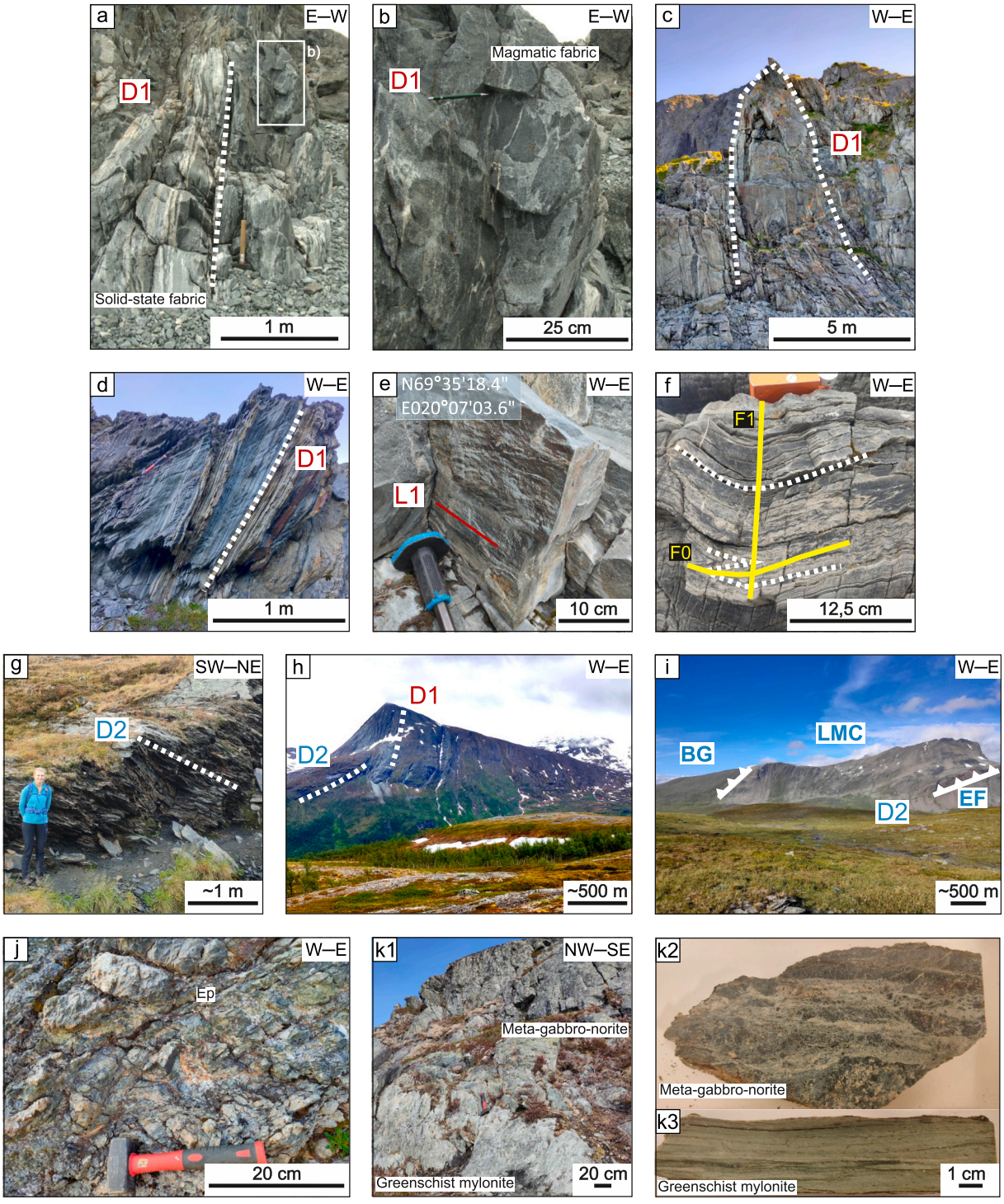

Fig. 9. Collection of field photographs. a) Magmatic and solid-stated deformed fabrics parallel to each other with steeply dipping foliation. West-side of Lyngstuva. b) Close-up image of the magmatic fabric. West-side of Lyngstuva. c) Steeply inclined isoclinal folds. Lyngstuva. d) Greenschist-facies, solid-state deformed D1 fabrics with steeply dipping foliation. East-side of Lyngstuva. e) Steeply foliation with subhorizontal N—S trending stretching lineation (L1). Road between Svensby and Lyngseidet. f) Cross-cutting fold relationships, F0 being refolded by F1. Balsfjord Group metasediments adjacent to the Lyngen Magmatic Complex at Lattervika. g) Garnet-bearing amphibolite with gently dipping foliation and NW—SE stretching lineation (D2). Perstinden. h) Superposition of D1 and D2 structures. Svensborgtinden. i) Variation of foliation dip from lower to upper contact on the southern portion of the Lyngen Magmatic Complex. Lagofjellet—Storvasstinden. j) Epidote-bearing rocks withing greenschist mylonites. Balsfjord Group adjacent to Piggtinden. k1) Transition from lesser deformed meta-gabbro-norite to greenschist mylonite fabrics by retrogression and strain increase. Rødaksla; k2 and k3) Samples of meta-gabbro-norite and greenschist mylonite cut parallel to the lineation for the same outcrop.

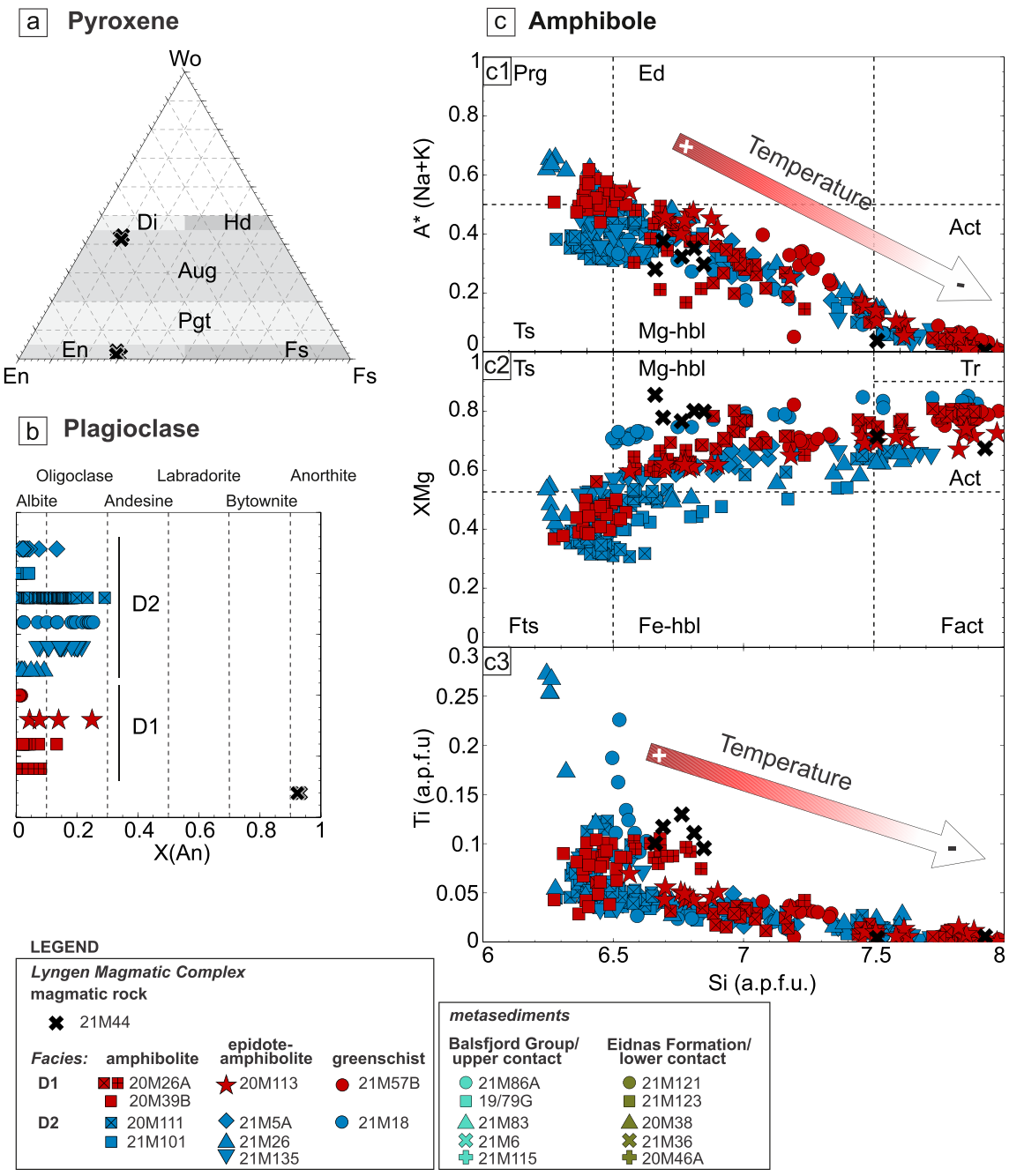

Fig. 10. a) Pyroxene classification for the magmatic fabric, the presence of both orthopyroxene and clinopyroxene makes it a gabbro-norite. b) Plagioclase distribution. The magmatic fabric contains An_{93} compositions, whereas retrogressed rocks present a range from albite to oligoclase (An_0—An_{29}). c) Amphibole classification. Samples collected from S1-L1 fabrics (red symbols) and S2-L2 fabrics (blue symbols) are classified into amphibolite (squares), epidote-amphibolite (D1: stars, D2: triangles, diamonds) and greenschist (circles) metamorphic facies. Black crosses represent undeformed rock and are used as a reference. c1) Decreasing trend for Na, and Ti from pargasite to actinolite, with some incursions into the edenite and tschermakite fields for S1-L1 and Ts for S2-L2. c2) Increasing trend for X_{Mg} from Fe-tschermakite to actinolite. Most samples show high Mg-ratios with decreasing from Fe-tschermakite to actinolite. Most samples show high Mg-ratios with decreasing metamorphic grade. c3) Decreasing trend of Ti-content with increasing Si content. Both D1 and D2 amphiboles show a transition from wider to tighter distribution towards lower temperatures. D2 samples associated to brown pargasitic cores present the highest Ti values. (For interpretation of the references to colour in this figure legend, the reader is referred to the web version of this article.)

between garnets could be either an effect of non-ideal sections through the garnet crystals or differences in the sample protolith. For instance, sample 21M6 was sampled from an area where a mixture of lithologies of the Balsfjord Group and mylonitic retrograded gabbro from the LMC is inferred. The garnet profile of this sample shares some similarities with the garnet profile of the LMC (20M111), with high spessartine and almandine content. However, some differences are also present, like lower Ca-contents compared to the garnet profile of the LMC. It is uncertain whether this sample might be related to the LMC. However, it is also distinct from the profile of the other Balsfjord sample (21M115).

The Balsfjord Group presents an inverse metamorphic gradient. The samples from this study include higher-grade Grt-bearing (21M6, 21M115) and biotite-bearing metapelites (21M86A) and lower-grade metasediments (19/79G, 21M83). In all cases, chlorite is similar to that of the Eidnas Formation (Fig. 6a) but with lower X_{Mg} except for sample 19/79G (0.57—0.61) (Fig. 6b). Higher-grade chlorite values

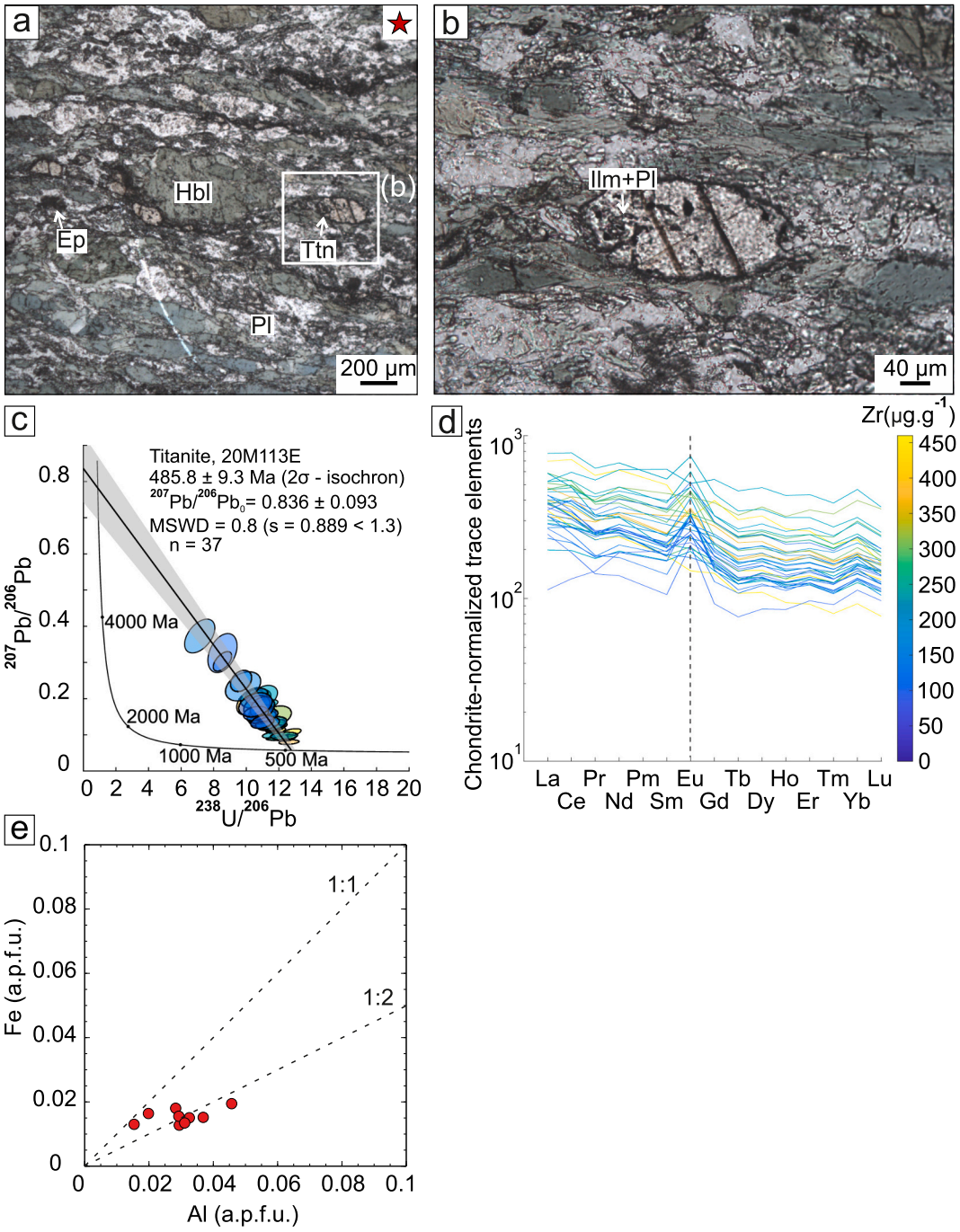

Fig. 11. a) Sample 20 M113 (dip direction/dip: 270/85; trend/plunge: 182/11) associated with D1 structures, where U—Pb dating of titanite was conducted. Shape preferred orientation of amphiboles and titanites are parallel to the stretching lineation (main fabric). b) close-up of a titanite grain containing inclusions of ilmenite and plagioclase. c) Tera-Wasserburg diagram and discordia date for titanites from derived titanite. In addition, there are 3 negative values for Eu anomaly, ranging from −0.35 to −0.09, and 8 values with small positive Eu anomaly ranging from 0.01 to 0.06. These values could suggest magmatic origin. d) Fe v. Al diagram for titanite. Most data fall on or under the 1:2 Fe:Al ratio indicating a metamorphic origin.

range from 0.48 to 0.62 (X_{Mg}) and 2.59 and 3.36 apfu (Si). In lower-grade rocks, chlorite compositions range from 0.48 to 0.58 in X_{Mg} and 2.62 to 2.83 Si apfu.

White mica analyses show muscovite with minor phengitic substitution (Fig. 6d). X_{Mg} values range from 0.26 to 0.49, except for sample 19/79G (0.63—0.73) (Fig. 6e). This range is lower than for the Eidnas Formation. Si contents vary between 2.80 and 3.32 apfu.

4.3.4. *Thermobarometry*

Table 2 presents peak metamorphic temperatures and their standard deviations (SD) obtained by Raman spectroscopy (RSCM) for 12 samples of the Balsfjord Group (contact with the LMC). Fig. 8 illustrates the temperature distribution in the area. Temperatures vary along strike and temperatures decrease towards the contact with the LMC. In the northern portion of the Lyngen Peninsula, samples 21M87 and 21M131 show higher temperature values (500 and 541 °C ± 50 °C) that also correspond with the presence of garnet in the samples. In this section,

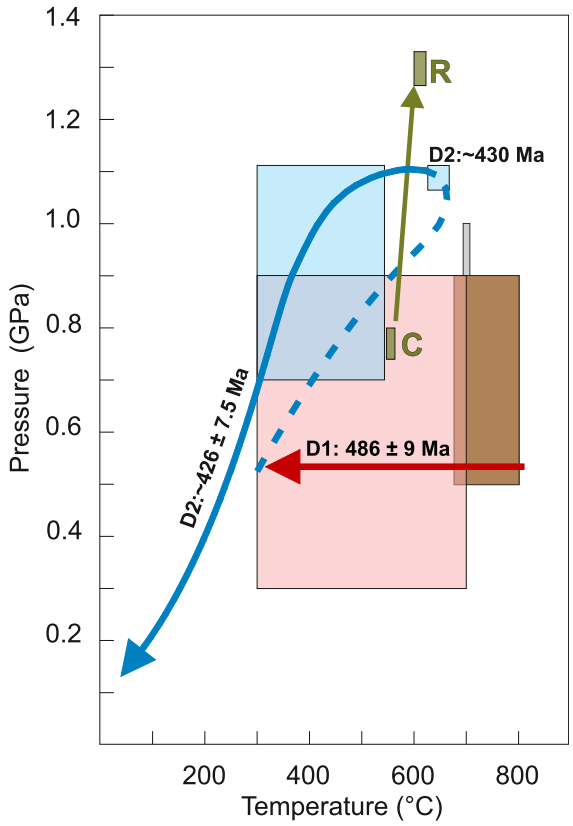

Fig. 12. Pressure-temperature evolution of the Lyngen Magmatic Complex. Two different deformation events occurred: D1 (in red), dextral strike-slip transpressional deformation during incipient formation of the Lyngen Magmatic Complex in a supra-subduction zone. D2 (in blue) is related to the Scandian episode during the formation of the North Norwegian Caledonian Nappe sequence. Data suggests that each event transitions from high to low temperature conditions, meaning that there was a reheating during initial stages of D2. An increase in pressure conditions accompanied this reheating event. Other P-T-conditions: in brown, anatectic tonalite from the Lyngen Magmatic Complex (Selbekk et al., 2002); green, prograde path from garnet-bearing metasediments from the Eidnas Formation (C: core, R: rim; this study); in grey, Scandian shearing for the Nordmannvik Nappe (Faber et al., 2019). (For interpretation of the references to colour in this figure legend, the reader is referred to the web version of this article.)

the closest sample to the LMC (i.e., 21M125) presents temperature values of 477 ± 50 °C. These mean temperatures are slightly higher than in the sample in the southern Lyngen Peninsula (i.e., 19/79G, 426 ± 50 °C), but overlapping within uncertainties. Chlorite thermometry of the samples of the Balsfjord Group yields a mean crystallization temperature of ~340 to 515 ± 50 °C (~450 ± 50 °C when considered together) (supplementary material).

5. Interpretations

The structural results from this study outline two deformation events, which both involve the formation of mineral assemblages during a transition from higher to lower temperature as demonstrated by amphibole zoning (i.e., trend in Si content) and albitization of plagioclase (Fig. 10). D1 corresponds to a transition from magmatic conditions through amphibolite-, epidote-amphibolite to greenschist facies metamorphism (reactions 1 to 3), followed by D2 from lower amphibolite to greenschist facies.

(1) Magmatic fabric ➔ Amphibolite facies:
Cpx + Opx + Pl_1 (An_{93}) + H_2O ➔ Amp_1 (Prg) + Qz + Pl_2 (An_{10-20}) + Ti-phase (Rt/Ilm) (± Bt, ± Grt).

(2) Amphibolite facies➔ Epidote-amphibolite facies:
Amp_1 (Prg) + Qz + Pl_2 (An_{10-20}) + Ti-phase (Rt/Ilm) + H_2O (± Bt, ± Grt) ➔ Amp_2 (Mhb) + Qz + Pl_3 (An_{0-10}) + Ti-phase (Ttn) + Ep

(3) Epidote-amphibolite facies ➔ Greenschist facies:
Amp_2 (Mhb) + Qz + Pl_3 (An_{0-10}) + Ti-phase (Ttn) + Ep + H2O ➔ Amp_3 (Act) + Qz + Pl_3 (An_{0-10}) + Ti-phase (Ttn) + Ep + Chl.

Not all samples include all the minerals listed in the generalized reactions above. The rocks from the LMC went through all three metamorphic stages during D1 and D2 events. Thus, it is not possible to distinguish the deformation phases based on metamorphic conditions. Significant re-heating of the rocks is required between D1 and D2 (Fig. 12).

During reaction 1, Ca from the magmatic plagioclase and clinopyroxene is incorporated into the formation of pargasite (Fig. 4c). Titanium from decomposing clinopyroxene is transferred to the Ti- phases (typically rutile or ilmenite). During reaction 2, pargasite retrogrades into Mg-hornblende and Na from the A site is incorporated into plagioclase. Titanium within pargasite grains exsolves and is incorporated into the Ti-rich phase (titanite). Calcium and Al from plagioclase are incorporated into epidote. During reaction 3, Mg-hornblende retrogrades to actinolite. During amphibole retrogression through reactions 2 and 3 $Al^{IV} \leftrightarrow Si^{4+}$ and $Al^{VI} \leftrightarrow$ (Mg, Fe) substitutions occur. Aluminium from amphibole is incorporated into chlorite.

For metapelitic rocks like the Eidnas Formation and Balsfjord Group, Mg-rich chlorite indicates higher metamorphic grades than Fe-rich chlorite (Zane et al., 1998). The difference between both high and lower grade chlorite is low but consistent with the metamorphic grade. In addition, the lower silicon range of the metapelitic chlorite may suggest higher temperature conditions than chlorite from the LMC (Zane et al., 1998). In white mica, Si content decreases with increasing temperature in the pyrophillitic substitution (Dubacq et al., 2010), suggesting overall higher crystallization temperatures for the Eidnas Formation compared to the Balsfjord Group.

5.1. P-T-t evolution during D1 along the LMC

Trace element analyses for sample 20M113 allowed to distinguish two titanite populations within the mylonitic and retrogressed gabbronorite, yielding a U—Pb date of 486 ± 9 Ma. The first population, characterized by a positive Eu anomaly (Fig. 11d), indicate titanite growth associated to the breakdown of (possibly magmatic) plagioclase, i.e. during solid-state overprint. In addition, titanite Fe/Al ratios between 0.4—0.5 are consistent with a metamorphic origin of titanite (Nakada, 1991; Kowallis et al., 2022), and titanite U—Pb dates have been shown previously to yield crystallization ages in amphibolite-facies metamorphism (e.g., Soret et al., 2022). Consequently, the U—Pb date is interpreted as representing the crystallization age of metamorphic titanite, as a product of the breakdown of pyroxene/ilmenite during retrograde metamorphism and deformation of the gabbro. The associated steeply dipping S1 foliation and sub-horizontal N—S-trending stretching lineation L1 clearly indicates that this deformation/metamorphic event corresponds to D1 (Fig. 9e). The strong shape-preferred orientation of titanite, amphibole as well as ilmenite and plagioclase included in titanite confirms/supports the *syn*-kinematic growth of the grains (Fig. 11b). Augland et al. (2014) established 481 ± 6 Ma as the crystallization age for tonalitic intrusions (magmatic age). Their age overlaps with the present metamorphic age of titanite suggesting a close association of magmatic and D1 metamorphic events. The overlapping ages are consistent with gradational transitions of magmatic and solid-state deformational structures and their same orientations in the field (Figs. 2, 3, and 9). Consequently, the D1 event appears partially

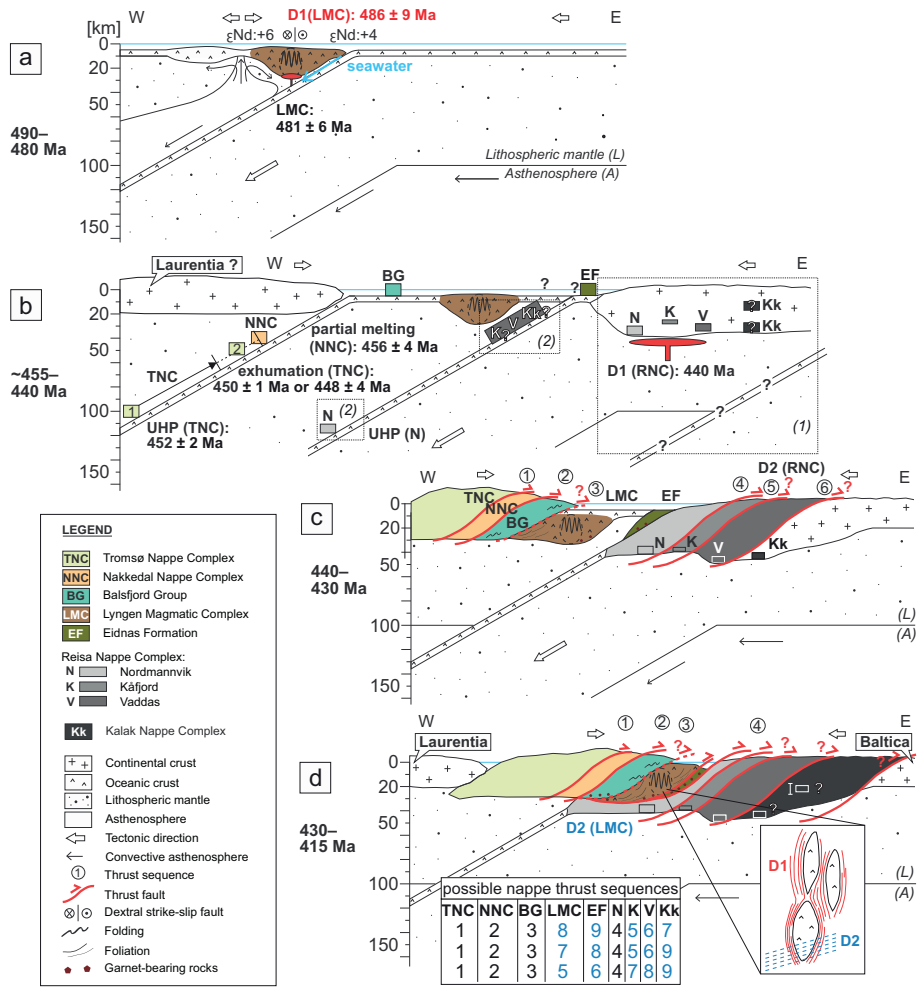

Fig. 13. a) 486 Ma, D1 event synchronous to incipient formation of the Lyngen Magmatic Complex above a subduction zone (Selbekk et al., 2002; Augland et al., 2014). D1 is characterized by a dextral strike-slip transpressional regime. b) Between ~455—440 Ma, the Tromsø and Nakkedal Nappe Complex were under UHP and HT conditions (respectively) while two possible scenarios are presented for the Reisa Nappe Complex (grey units). 1) This unit is going through its first metamorphic overprint. Relative position of each nappe is marked by a rectangle with letters (N, K, V, and Kk according to Faber et al., 2019). 2) UHP conditions for the Nordmanvikk Nappe as discussed by Janák et al. (2024). c) 440—430 Ma, Scandian collision; in-sequence nappe assembly at the west of the Lyngen Magmatic Complex is thrust on top of the Lyngen Magmatic Complex. The thickening of the upper nappe assembly brings the Lyngen Magmatic Complex to greater depths, increasing P-conditions to maximum values of 1.1 GPa. At this stage the Lyngen Magmatic Complex was positioned at the same depth as the Reisa Nappe Complex, with the Eidnas Formation located laterally between these units. The Eidnas Formation is transported to lower crustal levels forming prograde garnets (Schiffer, 2017; this study) and is positioned between hotter units above and below. d) 430—415 Ma, the continuing collision of the Caledonian Nappe sequence causes the thinning of the Lyngen Magmatic Complex in some regions of the body. In addition, local regions at the base of the Balsfjord Group are reheated. D2 structures form within the Lyngen Magmatic Complex.

magmatic and partially metamorphic. The indistinguishable ages suggest rapid cooling during structural evolution.

Peak P-T-conditions of the solid-state overprint within the metagabbro-norite (20M113) of the LMC estimated by conventional thermobarometry (650 ± 40 °C and 0.9 ± 0.15 GPa) are inconsistent with the results obtained from Zr-in-titanite thermometry (~690 ± 20 °C at 0.3 GPa; 760 ± 20 °C at 0.9 GPa). However, both values are in agreement with those from fluid inclusions reported in anatectic tonalite indicating peak P-T-conditions of 680—800 °C and pressures of 0.5—0.9 GPa (Selbekk et al., 2002). The metamorphic grade at the time of deformation provided by microstructural information indicates epidote-amphibolite facies, consistent with conventional thermobarometry and experimental data for the stability field of epidote (Apted and Liou, 1983; Deer et al., 1992). Therefore, the difference in values is most likely due to differences in the advancement of overprint between the titanite and the amphibole-plagioclase pairs during the retrograde P-T evolution. The rapid cooling during the D1 overprint concluded above would make it likely that differing T conditions can be preserved during the same structural event.

Pressure constraints of 0.9 GPa are too high for deformation in a typical ocean-floor setting (where pressures of ~0.2—0.3 GPa can be expected). Yet, the results from this study and those reported by Selbekk et al. (2002) are consistent with a location deeper in the crust than the conventional ocean floor ophiolite at the time of epidote-amphibolite facies overprint. This can be explained by a more complex back-arc situation, where transpressional movements can affect the depth of the magmatic rocks (e.g., Herwegh et al., 2016).

5.2. *P-T-t evolution during D2 along the Eidnas Formation, and Balsfjord Group*

Phase equilibrium modelling on Grt-bearing metasediments (21M123) from the Eidnas Formation (i.e., the unit directly below the LMC) yield conditions of 558 ± 8 °C, 0.8 GPa (garnet core), and 610 ± 10 °C, 1.3 GPa (garnet rim). These values are consistent with those reported by Schiffer (2017) (core: 525 °C, 0.75 GPa; rim: 600 °C, 1.0—1.1

GPa) reflecting prograde metamorphism (Schiffer, 2017; this study) without retrogression. The peak temperatures are also consistent with RSCM. Results yield an average peak T of ~535 °C ± 50 °C. The T conditions are also in agreement within uncertainties with described SGR + GBM microstructures in quartz (Fig. 4m). SGR microstructures in quartz develop between 400 and 500 °C (Lloyd and Freeman, 1994; Stipp et al., 2002), whereas GBM suggests higher temperature conditions (given similar strain rates) in the range 500–700 °C (Jessell, 1986; Stipp et al., 2002). The presence of plagioclase grains with albite cores and oligoclase rims (Fig. 4n and supplementary material), with epidote inclusions within Grt-porphyroblasts and absence of epidote in the matrix support the interpretation that this assemblage formed during prograde metamorphism in the Eidnas Formation. Garnet crystals from this unit most likely grew rapidly and were unaffected by diffusional relaxation, as shown by small grain sizes and well-developed zonation patterns in sample 21M123 (e.g., Florence and Spear, 1991). Chlorite thermometry in the Eidnas Formation shows decreasing temperature values towards the inner parts of the unit, with maximum temperatures close to the contact with the Reisa Nappe Complex (21M123; Fig. 6c and 8a). This observation is consistent with the interpretation of a cooler tectonic unit positioned between two warmer units.

The fact that the Eidnas Formation only records a prograde P-T-path indicates that it only underwent the Scandian phase (D2) and no earlier events. D1 structures in this unit are absent, and shear senses and orientations of the foliation and stretching lineation are consistent with D2 only. Thus, the Eidnas Formation neither records the D1 history of the LMC nor the earlier tectonic history of the Reisa Nappe Complex below (Faber et al., 2019). The lack of earlier deformation and metamorphic history likely indicates that the Eidnas Formation represents a slice of different rocks, most likely derived from a sedimentary unit of the Caledonian sedimentary cycle (unlike the pre-Caledonian units below, e.g., the Kalak Nappe; Gasser et al., 2015; Faber et al., 2019) and the pre-D1 LMC rocks (~480 Ma). This sedimentary unit is now positioned between higher temperature units above and below and shows lower temperatures in the inner parts of the unit than the contact rocks. Small temperature variations at the contact regions can be partly due to heat transfer from the LMC and the Reisa Nappe Complex.

The reported RSCM temperature conditions for the Eidnas Formation are above the closure temperature T_c for biotite (T_c = 450 °C; Reiners and Brandon, 2006) and white mica (i.e., phengite, T_c = 350 °C; Dahl, 1996) based on Ar diffusion. For this reason, the two dates of 424 ± 5 Ma (biotite) and 427 ± 10 Ma (white mica) are considered as cooling ages and, therefore, minimum formation ages for the low-grade minerals in this unit. The mica cooling ages in the Eidnas Formation overlap within uncertainties with the Scandian collision. Faber et al. (2019) reported 432 ± 6 Ma for the Scandian shearing at T = 700 °C along the boundary between the Kalak Nappe and the Vaddas Nappe (i.e., the deformation event in the Reisa Nappe Complex that should approximately correspond to the D2 event of this study). Considering the uncertainties of the 432 ± 6 Ma formation ages of the Reisa Nappe Complex and the 424 ± 5 Ma (biotite) and 427 ± 10 Ma (white mica) cooling ages of the Eidnas Formation, the age ranges overlap. This is consistent with rapid cooling after crystallization during/after Scandian thrusting (~430 Ma).

Peak conditions of 650 ± 40 °C and 1.1 ± 0.15 GPa for D2 estimated in the Grt-bearing amphibolite (20M111) located near the base of the LMC are consistent with the ones estimated for the late deformation event of the underlying Reisa Nappe Complex (i.e., Nordmannvik Nappe) during Scandian collision (D2: T = 700 °C, P = 0.9—1.0 GPa; Faber et al., 2019). For chlorite thermometry, lower crystallization temperatures appear more clearly in areas where the thickness of the LMC is greater, whereas thinner portions of the meta-gabbro-norite likely preserve higher temperature values. This suggests that the contacts of the thick LMC parts record later structural stages of the tectonic evolution on the established retrograde P-T path.

The metasediments of the Balsfjord Group on top of the LMC in the northern Lyngen Peninsula have the same orientation (lineation and foliation) as the meta-gabbro-norite of our D1 phase (486 ± 9 Ma). However, their age of less than 429 ± 5 Ma (Höpfl et al., 2024) further west is slightly younger than or overlapping with D2, i.e., Scandian deformation. Höpfl et al. (2024) have recently discussed the direct impact of the LMC on the development of Scandian structures in the Balsfjord Group. The complex folding history of folds with either steeply or gently inclined axial planes of the Balsfjord Group (D4 phase defined by Höpfl et al., 2024) is absent in the lower Reisa Nappe Complex, where low-angle dipping, shear-dominated structures are observed (Faber et al., 2019). The thrusting at the top of the LMC may have influenced the internal deformation of the Balsfjord Group. However, more detailed radiochronometric dating is needed to allocate the time of deformation of the metasediments of the Balsfjord Group, which could provide key information to better understand the relation between the LMC and the Balsfjord Group. No recent detailed study of the different lithologies and stratigraphy of this series has been carried out and, because of the Ullsfjord (Fig. 2a), there is a complete lack of outcrop of several kilometers between the northern Lyngen Peninsula and the series described by Höpfl et al. (2024) further west. This lack of information prevents us from making further interpretations. However, samples within the Balsfjord Group allocated in areas further south (e.g., Strupen or Vikafjellen, Fig. 2a) show clear orientations corresponding to D2 of this study (e.g., sample 19/79G, Table 1; and stereoplot sG2, Fig. 2a and b). Thus, RSCM and chlorite thermometry values for these regions reflect temperatures that prevailed during the D2 Scandian event on top of the LMC. The distribution of chlorite crystallization temperatures (Fig. 6c and 8a) is unclear. Values vary between 420 and 460 °C at approximately the same tectonostratigraphic level. This variation is within the error of the method, so it is difficult to establish whether a decrease in temperatures from north to south really exists, as suggested in Fig. 8a.

For the Eidnas Formation, LMC and Balsfjord Group, chlorite thermometry yields two different temperature ranges (LT from 300 to ~400 °C and HT from ~400 to ~650 °C; Table 2 and supplementary material), with a substantial variability of temperature estimates (Fig. 6c and 8a). Two temperature ranges are often observed in zoned chlorite (e.g. Vidal et al., 2006), possibly linked to modelling artefacts, calling for caution. Pressure conditions for the D2 retrogression of the metasediments of the Balsfjord Group and Eidnas Formation remain poorly constrained (Fig. 12). Low celadonite and pyrophyllite contents (Fig. 6d) are consistent with greenschist facies conditions.

Integrating geographical distribution of RSCM results, Grt-amphibolite thermobarometry, and phase equilibrium modelling (Fig. 8b) reveals a progressive decrease in temperature conditions during Scandian thrusting (D2), from ~425 °C in the Balsfjord Group towards the tectonic contact between the LMC and Nordmannvik Nappe at ~430 Ma (Fig. 8b). A decrease in temperature from the Nordmannvik to the Kalak Nappe Complex is also reported at ~430 Ma (Faber et al., 2019; Yogi et al., 2024) (Fig. 8b). $^{40}Ar/^{39}Ar$ data from the Tromsø Nappe suggests T-conditions of 500 to 375 °C between 433 ± 11 and 437 ± 16 Ma (Krogh et al., 1990) or 427 and 410 Ma (Dallmeyer and Andresen, 1992). Therefore, the Tromsø Nappe was already emplaced at upper crustal levels at ~430 Ma, consistent with in-sequence thrusting and emplacement of the Tromsø Nappe on top of the Nakkedal Nappe and Balsfjord Group and subsequently onto the LMC (at progressively higher structural levels in the crust). Within the LMC, the maximum D2 temperature reaches ~650 °C. Temperatures progressively decrease towards the Eidnas Formation (~530 to 610 °C) and increase again to ~700 °C in the Reisa Nappe Complex (Nordmannvik Nappe; Faber et al., 2019) (Fig. 8b). The temperature difference between the LMC and the Eidnas Formation and the temperature gradient within the Eidnas Formation likely suggest an out-of-sequence relationship between LMC, Eidnas Formation, and Nordmannvik Nappe. Locally, the main D2 movements may have been followed by local late extensional movements with top-to-the-NW as suggested by late S-C′ fabrics in the Eidnas Formation (21M121, 21M123; Fig. 3d3). It is noteworthy that maximum

D2 pressure and temperature conditions in the LMC during the Scandian event (650 ± 40 °C and 1.1 ± 0.15 GPa) are lower than early (740—770 °C, 1.3—1.5 GPa at 448 ± 2 Ma; Dallmeyer and Andresen, 1992; Janák et al., 2012) and higher than late (500—375 °C, <0.8 GPa at ~440—430 Ma; Krogh et al., 1990; Dallmeyer and Andresen, 1992) exhumation P-T conditions in the Tromsø Nappe Complex (tectonically above the LMC and Balsfjord Group).

6. Regional-scale integration of the LMC evolution and surrounding nappes

6.1. Oceanic pre-collisional structures (D1)

New field data reveal that the northern portion of the Lyngen Peninsula (Fig. 1b) is dominated by penetrative D1-structures with steeply inclined foliation, subhorizontal stretching lineation, isoclinal folds, and dextrally sheared mafic units associated with a strike-slip transpressional regime (west-block transported to the north; Fig. 3c). These structures affect large parts of the LMC to a different extent and are not just restricted to a single discrete local shear zone (i.e., the Rypdalen Shear Zone) as suggested by previous work (Furnes and Pedersen, 1995; Slagstad, 1995a, 1995b). Field observations from this study across several transects along the LMC indicate variably deformed fabrics with only local occurrences of undeformed lenses. In addition, a direct relationship of magmatic and high temperature solid-state structures (Fig. 9a, b, and d) is established at Lyngstuva (northern Lyngen Peninsula). There, the presence of magmatic and metamorphic fabrics with the same orientation (S1-L1) and a gradual transition from magmatic to solid-state fabric indicate rapid development of high temperature solid-state structures after magmatic emplacement of the LMC during the D1 event. This field observation is confirmed by the overlapping titanite ages of 486 ± 9 Ma for the solid-state overprint (this study) and the magmatic ages of 481 ± 6 Ma (Augland et al., 2014). Slagstad et al. (2020) recently questioned the interpretation of the LMC magmatic ages (Oliver and Krogh, 1995; Augland et al., 2014) for being younger than the 494 ± 5 Ma felsic veins intruding the Lillevik ophiolite (Gratangseidet Igneous Complex in Narvik). Similar age values are observed in other ophiolites along the Norwegian Caledonides (Slagstad et al., 2020). Although younger, the results of this study partly overlap the ages reported by Slagstad et al. (2020) and suggest that the age of 481 ± 6 Ma (Augland et al., 2014) might be lower than expected and represent minimum crystallization values. D1 deformation is interpreted to take place in an oceanic crustal setting during back-arc spreading above a subduction zone, similar to settings in Oman (Slagstad, 1995a, 1995b; Dilek and Flower, 2003; Kvassnes et al., 2004, Fig. 13a). P-T estimates at the base of the ophiolite from fluid inclusions in anatectic tonalite determine maximum temperature conditions of 680—800 °C and pressures of 0.5—0.9 GPa (Selbekk et al., 2002). Subsequently, progressive cooling occurred at constant pressure to epidote-amphibolite (650 °C, 0.9 GPa) and P-T conditions decreased at greenschist facies (~300—450 °C and 0.3—0.75 GPa) as indicated by the retrograde mineral assemblage (Table 1; Fig. 4d).

After D1, there is an extended transition period of 50 Ma until the Scandian collision (D2), for which no rock record has been identified in the study area. At 455—440 Ma, the Tromsø and Nakkedal nappes are known to have reached high temperature (Selbekk et al., 2000; Ravna and Roux, 2006; Ravna et al., 2006) and (ultra)high-pressure (UHP) metamorphic conditions (Ravna and Roux, 2006; Fassmer et al., 2020, and references therein), with the Tromsø Nappe Complex buried at maximum depths of ~105–123 km (3.2–3.5 GPa; Ravna and Roux, 2006; Janák et al., 2012) at 452.1 ± 1.7 Ma (Corfu et al., 2003) possibly under Laurentian margin (Roberts et al., 2007 and references therein) (Fig. 13b). At 450.3 ± 0.9 Ma (Corfu et al., 2003) the Tromsø Nappe experienced partial melting at 760–845 °C and 2.0–2.2 GPa (Ravna and Roux, 2006). Later, both units were exhumed and cooled (Coker-Dewey et al., 2000; Corfu et al., 2003; Ravna and Roux, 2006; Janák et al., 2012; Augland et al., 2014) in a setting further west, outboard of the LMC (Fig. 13b and c). Several authors interpreted that the juxtaposition of the Tromsø Nappe onto the Nakkedal Nappe took place at P-T conditions of >750 °C and 1.0 GPa (Krogh et al., 1990; Ravna and Roux, 2006; Ravna et al., 2006; Fassmer et al., 2020). Titanite dating of post-eclogitic leucosomes within the Tromsø Nappe yield ages of 450 ± 1 Ma interpreted as cooling and uplift of the unit after UHP conditions (Ravna and Roux, 2006). The range of the subduction-exhumation cycle of the Tromsø Nappe has recently been estimated between 454.5 ± 1.1 and 448.8 ± 1.4 Ma (Fassmer et al., 2020). These results are consistent with the interpretation of fast subduction and exhumation for the same unit (452—449 Ma, Corfu et al., 2003). Isotope correlation ages from $^{40}Ar/^{39}Ar$ geochronology in hornblende of the Tromsø Nappe suggests diachronous cooling between 452 and 432 Ma (Dallmeyer and Andresen, 1992). Migmatization of the Nakkedal Nappe has been dated with U—Pb on titanite, yielding an age of 456 ± 4 Ma (Selbekk et al., 2000).

Towards the east, at the inboard side of the LMC, the Reisa Nappe Complex was going through the first metamorphic event (D1) described for this unit by Faber et al. (2019). This event in the Reisa and Kalak nappes is characterized by magmatic underplating at deep levels of the continental crust (~440 Ma; Faber et al., 2019) above another potential subduction zone further to the East (Fig. 13b). Estimated depths for the units are: ~30—37 km (with partial melting; Nordmannvik Nappe), ~20—26 km (Kåfjord Nappe), and ~26—34 km depth (Vaddas Nappe) (Elvevold, 1988; Lindstrøm and Andresen, 1992; Faber et al., 2019). Similar timing of metamorphic grade locates the Kalak Nappe Complex at comparable depths to the Reisa Nappe Complex between 445—440 Ma (Ziemniak et al., 2019). Alternatively, the upper units of the Kalak Nappe Complex could have been at shallower depths of 14—16 km (0.45 GPa) at 464 Ma evidencing internal out-of-sequence thrusting during the Scandian phase (Gaidies et al., 2021). The Eidnas Formation probably represents a marine sedimentary cover at some quiet structural setting (Fig. 13b) because a D1 event is not observed in this unit, and later D2 structures and metamorphic overprint only record prograde P-T-conditions. Alternatively, the presence of microdiamonds and melt inclusions within the Nordmannvik Nappe (Heia locality, Fig. 2a) in combination with Zr-in-rutile analyses suggest that the unit was transported to deep crustal levels reaching minimum P-T conditions of 840—870 °C and 3.7—3.8 GPa (Janák et al., 2024). Although geochronological data for such an event is missing, Janák et al. (2024) allocate the timing of the UHP event of the Nordmannvik Nappe as pre-Scandian based on foliation overprinting relations. This new scenario suggests that the Baltica margin subducted in an arc-continent collision setting, raising new questions regarding the tectonic evolution of the Nordmannvik Nappe before the Scandian collision. Studies from the same locality (Heia, Fig. 2a) describe a 492 ± 5 Ma metadiorite (Lindstrøm and Andresen, 1992) interpreted as a protolith of an upper amphibolite-granulite mylonitic gneiss showing prograde metamorphism at 715 ± 30 °C and 0.9 ± 0.1 GPa (Elvevold, 1988). This interpretation could potentially allocate the UHP conditions of Janák et al. (2024) to a pre-Caledonian stage, certainly earlier than depicted in Fig. 13b. The presence of UHP in the Nordmannvik opens another question regarding the tectonic evolution of the Kåfjord, Vaddas, and Kalak Nappes, which do not exhibit signs of UHP conditions. For instance, the Kåfjord Nappe (underneath the Nordmannvik Nappe) exhibits peak P-T conditions at 680—720 °C and 0.8—1.0 GPa during prograde phase of migmatization between 444±12 Ma and 442±6.5 Ma (Ziemniak et al., 2019). Determining if these units were subducted to shallower crustal levels goes beyond the scope of this project but is a scenario worth exploring in future studies.

The tectonostratigraphic framework of the Caledonides collected in the 1985 special publication (e.g., Roberts and Gee, 1985) has shown, over time, to present challenges when ascribing structural position to continental affinity (Corfu et al., 2014). Fig. 13b suggests that the subduction of the Tromsø and Nakkedal nappes could have occurred under the Laurentian margin based on the interpretation that the LMC marks

the limit between Baltica and Laurentian terrains (e.g., Gee et al., 2014). Slagstad and Kirkland (2017) considered that the ophiolitic bodies in Norway might not represent Scandian sutures (i.e., the tectonic contact between Baltica- and Laurentia-derived units) and proposed alternative models for the progression of the collision. These alternative models reconcile with those studies that interpret the Uppermost Allochthon of Northern Norway to be the equivalent of the high-grade units of the Seve Nappe Complex in the Jämtland area (i.e., outermost margin of Baltica, Middle Allochthon) (e.g., Janák et al., 2012). The palinspastic reconstruction of the Tromsø and Nakkedal nappes is not clear yet, and additional studies should address this topic.

6.2. Scandian thrusting (D2)

The LMC has been affected by a second deformational event (D2) reflecting the typical top-to-the-SE-transport direction for Caledonian nappe thrusting during Scandian collision (~430 Ma; Faber et al., 2019; Fig. 13c and d). D2 structures are dominant in the southern portion of the Lyngen Peninsula (Fig. 1b). Therefore, preservation of deformation events shows a transition from older to younger from north to south along the Lyngen Peninsula. The overprinting relationships between older D1 and younger D2 structures mark a large-scale boudin-type geometry of the LMC (Fig. 13d). Amphibole-plagioclase thermobarometry reveals that D2 occurred during or after an increase in P-T conditions from ~300—450 °C and 0.3—0.75 GPa during D1 to 650 °C and 1.1 GPa during D2 at the base of the LMC (Fig. 12). Thus, indicating reheating and pressure increase between D1 and D2. During Scandian thrusting, D1 structures were progressively overprinted inside the LMC (especially close to the lower contact of the LMC). Additional thinning of the boudin-type body of the LMC has also occurred during D2 (Fig. 13d), as reflected by the enormous thinning of the LMC south and west of Nordkjosbotn (Fig. 2a). Therefore, the originally steeply oriented isoclinal folds generated during D1 are consistently re-oriented into a W-dipping foliation at dip angles varying from ~36—51° on average. D2 structures in the LMC are subparallel to those of the underlying Eidnas Formation and Reisa Nappe structures that have formed during Scandian thrusting and collision (Faber et al., 2019). After reaching D2 maximum P-T-conditions the LMC rocks retrograded (lowering P and T) during top-to-the-SE-directed Scandian thrusting to progressively shallower structural levels.

Faber et al. (2019) suggested that at 432 ± 6 Ma the units within the Reisa Nappe Complex (i.e., lower nappe stack) were thrusted in-sequence during the D2 event described for this unit (Fig. 13c). According to their P-T estimations, the D2 structural position for the units are: ~35—41 km (Nordmannvik Nappe), ~36—39 km (Kåfjord Nappe), and ~44—48 km depth (Vaddas Nappe). Additional thermochronological studies (Kirkland et al., 2021) suggested peak temperatures of 630 °C at ~433 Ma with a low residence time (~5 Ma) for the lower units compared to the upper units of the Kalak Nappe Complex. This age is interpreted to reflect Scandian fabric generation at or near peak metamorphism (Kirkland et al., 2021). In this case, the LMC and Eidnas Formation could have been emplaced after the Kåfjord Nappe but before the Kalak Nappe Complex (Fig. 13d). Pressure conditions of the highest unit of the Reisa Nappe Complex (Nordmannvik: 700 °C, 0.9–1.0 GPa; Faber et al., 2019) are consistent with those of the base of the LMC during D2 (1.1 GPa). The structural or crustal depth must have been similar for the LMC and the Reisa Nappe Complex judging from the temperature and pressure at the base of the LMC during D2 of amphibolite facies (650 °C, 1.1 GPa) and the Nordmannvik Nappe. In the lower nappe stack, late monazite growth at 419 ± 8 Ma and 416 ± 6.9 Ma suggests the Kåfjord Nappe to be emplaced at later stages of the Scandian phase (Ziemniak et al., 2019). Lower in the nappe stack, the Kalak Nappe Complex presents a polymetamorphic history at different tectonostratigraphic levels of the unit (Gaidies et al., 2021). Yogi et al. (2024) constrained peak P-T conditions of 630 °C and 0.7 GPa at 419.9 ± 2.4 Ma in the upper levels of the Kalak Nappe. This age agrees with the age for the emplacement of the Kåfjord Nappe by Ziemniak et al. (2019). Yogi et al. (2024) also identified a second generation of garnets overgrowing the main Scandian foliation that yield ages of 423 ± 1.9 Ma, interpreted as a metamorphic event resulting from repeated loading-unloading cycles during the Scandian phase. These results suggest that the Kåfjord Nappe and Kalak Nappe Complex could have been emplaced after the LMC and Eidnas Formation (Fig. 13d). As these units are part of the lower nappe stack, further detailed discussions are beyond the scope of this study.

While the LMC and the Reisa Nappe Complex were at a similar structural depth before the final part of the Scandian collision, the Eidnas Formation experienced prograde metamorphism during D2 as suggested by phase equilibrium modelling (Schiffer, 2017; this study, Fig. 5b and c). The Eidnas Formation reached a maximum of ~558 to 610 °C as the *syn*-kinematic temperature, much less than the LMC and the Nordmannvik Nappe (at least 50 to 100 °C warmer). The Eidnas Formation has had a paleogeographic position between the two complexes and presumably at higher structural level (Fig. 13c). The discrepancy of temperatures can be explained by a more outboard position of the LMC during its emplacement onto some structural depth similar to the Reisa Nappe Complex. During the final collision stage, the LMC and the overlying units came to lie above all lower nappe units placing the Eidnas Formation between the LMC and the Nordmannvik Nappe. $^{40}Ar/^{39}Ar$ dating of micas of the Eidnas Formation yields results of 426 ± 7.5 Ma. This age falls in line with those for the Tromsø Nappe (~427–410 Ma) and Balsfjord Group and Nordmannvik Nappe (~431–410 Ma) interpreted as post-Scandian metamorphic cooling result of the transport of these units to higher crustal levels during Scandian thrusting (Dallmeyer and Andresen, 1992). The Tromsø Nappe possibly underwent temperatures varying from 650 °C (Krogh et al., 1990) to possibly >375 °C (Dallmeyer and Andresen, 1992) (Fig. 8b). The present model also implies a tectonic contact between the Balsfjord Group andthe LMC, as opposed to previous studies (Minsaas and Sturt, 1985; Andresen and Bergh, 1985).

At this stage, the most highly deformed sections of the LMC are thinned by shearing up to ca. 99.4 %, reducing the distance between the Balsfjord Group and Nordmannvik Nappe. As a result of the strong thinning of some areas of the LMC, there occurs a re-heating at the base of the Balsfjord Group when the units are emplaced on top of the hot Nordmannvik Nappe. The re-heating is demonstrated by the presence of garnet within the Balsfjord Group metasediments adjacent to the thinned sections of the LMC south and west of Nordkjosbotn (i.e., Strupen area). Some degree of intermixing between the LMC and Balsfjord Group could have occurred in these deeper sections. RSCM values of the Balsfjord Group rocks show lower temperatures and no garnet towards the north of the Lyngen Peninsula, where the thickness of the LMC is greater. This temperature distribution is consistent with increasing metamorphic gradient towards the W—NW (Andresen et al., 1985; Coker-Dewey et al., 2000; Menegon and Fagereng, 2021; Höpfl et al., 2024), suggesting that increasing temperatures are caused by the contact between Balsfjord Group and Reisa Nappe Complex. The latest movements related to the retrogression of the rocks occurred between ~440 °C for the Eidnas Formation, ~475 °C for the LMC, and ~450 °C for the Balsfjord Group. Fig. 13d illustrates the final geometry of the nappe assemblage of the Northern Norwegian Caledonides with the UHP and HT units of the Tromsø and Nakkedal nappes exhumed to the uppermost positions of the sequence. Final exhumation of the Tromsø and Nakkedal nappes may have occurred during prograde metamorphism of the Balsfjord Group around 432 Ma (Coker-Dewey et al., 2000; Höpfl et al., 2024). During in-sequence thrusting, temperatures and pressures decreased in the Tromsø and Nakkedal Nappes from high pressures (Tromsø Nappe) and high temperatures (Nakkedal Nappe) to lower P-T-conditions corresponding to some level of the upper crust (Balsfjord Group) (Coker-Dewey et al., 2000; Corfu et al., 2003; Janák et al., 2012).

Some unclear aspects remain. For instance, rare top-to-the-W shear senses are locally associated with D2 (Fig. 3d2 and 3d3). This sense of

shear could be the results of either reoriented shear senses due to folding or perhaps formed by post-orogenic extensional movements.

The case of the LMC resembles that of the Eide lens in the Kalak Nappe Complex, which preserves both pre- (Neoproterozoic) and syn-Scandian deformation and metamorphism (Gasser et al., 2015). In both cases, the Scandian metamorphic overprint depends on the availability of fluids, which limits and controls the development of collisional structures. The pre-Scandian history of the LMC, characterized by transpressional movements (D1), facilitated the weakening of the magmatic gabbro-norite. Those areas affected by higher fluid-rock interactions were more susceptible to deform during the latter Scandian phase (D2), causing stain localization and facilitating major thinning of an otherwise rheologically competent lithology. Consequently, the thicker portions of the LMC have remained as a mechanically strong lens, largely escaping structural and metamorphic overprint during D2. Transpressional movements might not be uncommon above back-arcs and should be considered in polymetamorphic and deformation studies of ophiolitic bodies.

7. Conclusions

Using a combination of petrochronological, geochemical, and structural analyses, this study provides a new integrated model of the evolution of the Lyngen Magmatic Complex (LMC) of the North Norwegian Caledonides. Specifically, the tectono–metamorphic history is reconstructed representing an exceptionally well-preserved case of pre-collisional strike-slip structures of a back-arc crust. The new results highlight the existence of a D1 pre-collisional event characterized by dextral strike-slip transpressional deformation generating subvertical structures at 486 ± 9 Ma followed by a D2 Scandian collisional event generating low-angle-dipping structures. Reheating between both tectonic events occurred after D1 metamorphic retrogression of solid-state deformation from amphibolite to greenschist facies. The D2 event also occurred during a retrograde event. Similar D2 peak P-T conditions between the LMC (650 ± 40 °C, 1.1 ± 0.15 GPa; this study) and lower Nordmannvik Nappe (700 °C, 0.9–1.0 GPa; Faber et al., 2019) suggests that the reheating took place during nappe stacking of the Scandian collision. The Eidnas Formation located between LMC and Nordmannvik Nappe, however, only records prograde metamorphism (from 558—610 ± 10 °C, 0.8—1.3 GPa) with maximum RSCM temperatures of ~535 °C ± 50 °C. $^{40}Ar/^{39}Ar$ dating and P-T distribution across units indicate out-of-sequence thrusting at the base of the LMC and the Eidnas Formation between 425 ± 5 Ma and 427 ± 10 Ma.

Moreover, this study demonstrates that strain localization and partitioning in mafic rocks developed only where fluid infiltration occurred, controlling and limiting the structural and metamorphic overprint. A similar case has been described in the Kalak Nappe Complex (Gasser et al., 2015). However, unlike the Kalak Nappe, larger regions of the LMC have escaped collisional structural and metamorphic overprint and have remained as a mechanical strong body, possibly influencing on the development of folding of the overlying unit (Balsfjord Group; Höpfl et al., 2024). Therefore, this study serves as a unique example of how strain localization and partitioning affect the rheological evolution of a mafic crust, from seafloor spreading to demise in collisional orogens.

CRediT authorship contribution statement

Marina Galindos-Alfarache: Writing – review & editing, Writing – original draft, Visualization, Validation, Project administration, Methodology, Investigation, Funding acquisition, Formal analysis, Data curation, Conceptualization. **Holger Stünitz:** Writing – review & editing, Validation, Supervision, Resources, Project administration, Methodology, Investigation, Funding acquisition, Conceptualization. **Mathieu Soret:** Writing – review & editing, Validation, Methodology, Investigation, Formal analysis. **Guillaume Bonnet:** Writing – review & editing, Visualization, Validation, Investigation, Formal analysis, Data curation. **Benoît Dubacq:** Writing – review & editing, Validation, Software, Resources. **Morgan Ganerød:** Writing – review & editing, Visualization, Validation, Investigation, Formal analysis, Data curation.

Declaration of competing interest

The authors declare that they have no known competing financial interests or personal relationships that could have appeared to influence the work reported in this paper.

Acknowledgments

This work is part of a PhD project funded by the UiT-The Arctic University of Norway. Part of the support for the Raman spectroscopy and analytical work came from by The Research Council of Norway through the funding to The Norwegian Research School on Dynamics and Evolution of Earth and Planets, project number 249040/F60. The Research Council of Norway is also acknowledged for support to the Goldschmidt Laboratory national infrastructure (project number 295894). M. Galindos-Alfarache thanks A. Lee for field assistance, J. Konopásek for his help with $^{40}Ar/^{39}Ar$ geochronology and parts of the analytical work, and S. Höpfl for providing five samples from the Balsfjord Group for RSCM. J. Konopasek and S. Höpfl are also thanked for their constructive discussions on many issues. Special thanks to N. Rividi and M. Fialin for their assistance during EMPA data collection at CAMPARIS, M. Button for his assistance with LA-ICP-MS, and H. Furnes for his help providing old un-digitized literature. We would also like to thank B.E. Sørensen and an anonymous reviewer for their constructive comments that improved the presentation of our work.

Appendix A. Supplementary data

Supplementary data to this article can be found online at https://doi.org/10.1016/j.tecto.2025.230706.

Data availability

Data will be made available on request.

References

Agard, P., Soret, M., Bonnet, G., Ninkabou, D., Plunder, A., Prigent, C., Yamato, P., 2023. Subduction and Obduction Processes: the Fate of Oceanic Lithosphere Revealed by Blueschists, Eclogites, and Ophiolites. In: Catlos, E.J., Çemen, I. (Eds.). Compressional Tectonics: Plate Convergence to Mountain Building, Geophysical Monograph 277, First Edition. https://doi.org/10.1002/9781119773856.ch2.

Andresen, A., Bergh, S., 1985. Stratigraphy and tectonometamorphic evolution of the Ordovician—Silurian Balsfjord Group, Lyngen Nappe, North Norwegian Caledonides. In: Gee, D.G., Sturt, B.A. (Eds.), The Caledonide Orogen –Scandinavia and Related Areas. John Wiley and Sons Ltd., pp. 579–592

Andresen, A., Steltenpohl, M.G., 1994. Evidence for ophiolite obduction, terrance accretion and polyorogenic evolution of the north Scandinavian Caledonides. Tectonophysics 231, 59–70. https://doi.org/10.1016/0040-1951(94)90121-X.

Andresen, A., Fareth, E., Bergh, S., Kristensen, S.E., Krogh, E., 1985. Review of Caledonian lithotectonic units in Troms, North Norway. In: Gee, D.G., Sturt, B.A. (Eds.), The Caledonide Orogen –Scandinavia and Related Areas. John Wiley and Sons Ltd., pp. 569–578

Apted, M.J., Liou, J.G., 1983. Phase relations among greenschist, epidote-amphibolite, and amphibolite in a basaltic system. Am. J. Sci. 283 (A), 328–354.

Augland, L.E., Andresen, A., Gasser, D., Steltenpohl, M.G., 2014. Early Ordovician to Silurian evolution of exotic terranes in the Scandinavian Caledonides of the Ofoten–Troms area – terrane characterization and correlation based on new U–Pb zircon ages and Lu–Hf isotopic data. Geol. Soc. Lond. Spec. Publ. 390 (1), 655–678. https://doi.org/10.1144/SP390.19.

Bergh, S., 1980. Stratigrafiske, strukturgeologiske og metamorfe undersøkelser av kaledonske bergarter vest for Balsfjord i Troms. Unpublished cand. real. thesis. University of Tromsø, 168pp.

Bergh, S., Andresen, A., 1985. Tectonometamorphic evolution of the allochthonous Caledonian rocks between Malangen and Balsfjord, Troms, North Norway. Nor. Geol. Unders. 401, 1–34.

Beyssac, O., Goffé, B., Chopin, C., Rouzaud, J.N., 2002. Raman spectra of carbonaceous material in metasediments: a new geothermometer. J. Metamorph. Geol. 20, 859–871. https://doi.org/10.1046/j.1525-1314.2002.00408.x.

Binns, R.E., 1978. Caledonian nappe correlation and orogenic history in Scandinavia north of lat 67°N. Geol. Soc. Am. Bull. 89, 1475–1490. https://doi.org/10.1130/0016-7606(1978)89<1475:CNCAOH>2.0.CO;2.
Binns, R.E., Matthews, D.W., 1981. Stratigraphy and structure of the Ordovician—Silurian Balsfjord Supergroup, Troms, North Norway. Nor. Geol. Unders. 365, 39–54.
Bjørlykke, A., Olaussen, S., 1981. Silurian sediments, volcanics and mineral deposits in the Sagelvvatn area, Troms, Northern Norway. Nor. Geol. Unders. 365, 39–54.
Brown, M., 2009. Metamorphic patterns in orogenic systems and the geological record. Geol. Soc. Lond. Spec. Publ. 318 (1), 37–74. https://doi.org/10.1144/SP318.2.
Brown, D., Spadea, P., Puchkov, V., Alvarez-Marron, J., Herrington, R., Willner, A.P., Hetzel, R., Gorozhanina, Y., Juhlin, C., 2006. Arc-continent collision in the Southern Urals. Earth Sci. Rev. 79, 261–287. https://doi.org/10.1016/j.earscirev.2006.08.003.
Casey, J.F., Dewey, J.F., 1984. Initiation of subduction zones along transform and accreting plate boundaries, triple junction evolution and spreading centres—Implications for ophiolitic geology and obduction. In: Gass, I.G., Lippard, S. J., Shelton, a.W. (Eds.). Ophiolites and Oceanic Lithosphere. Geol. Soc. Lond. Spec. Publ. 13, 269–290. https://doi.org/10.1144/GSL.SP.1984.013.01.22.
Chroston, P.N., 1972. A gravity profile across Lyngenhalvøya, Troms, northern Norway. Nor. Geol. Tidsskr. 52, 295–303.
Cocks, L.R.M., Torsvik, T.H., 2002. Earth geography from 500 to 400 million years ago: a faunal and palaeomagnetic review. J. Geol. Soc. Lond. 159 (6), 631–644. https://doi.org/10.1144/0016-764901-118.
Coker-Dewey, J., Steltenpohl, M.G., Andresen, A., 2000. Geology of western Ullsfjord, North Norway, withemphasis on the development of an inverted metamorphic gradient at the top of the Lyngen Nappe complex. Nor. Geol. Tidsskr. 80, 111–127. https://doi.org/10.1080/002919600750042609.
Corfu, F., Ravna, E.J.K., Kullerud, K., 2003. A late Ordovician U-Pb age for the Tromsø Nappe eclogites, Uppermost Allcohton of the Scandinavian Caledonides. Contrib. Mineral. Petrol. 145, 502–513. https://doi.org/10.1007/s00410-003-0466-x.
Corfu, F., Andersen, T.B., Gasser, D., 2014. The Scandinavian Caledonides: main features, conceptual advances and critical questions. In: Corfu, F., Gasser, D., Chew, D.M. (Eds.). New Perspectives on the Caledonides of Scandinavia and Related areas. Geol. Soc. Lond. Spec. Publ. 390, 9–43. https://doi.org/10.1144/SP390.25.
Dahl, P.S., 1996. The crystal-chemical basis for Ar retention in micas: inferences from interlayer partitioning and implications for geochronology. Contrib. Mineral. Petrol. 123, 22–39. https://doi.org/10.1007/s004100050141.
Dallmeyer, R.D., Andresen, A., 1992. Polyphase tectonothermal evolution of exotic Caledonian nappes in Troms, Norway: evidence from 40Ar/39Ar mineral ages. Lithos 29, 19–42. https://doi.org/10.1016/0024-4937(92)90032-T.
Deer, W.A., Howie, R.A., Zussman, J., 1992. An Introduction to the Rock-Forming Minerals, Second edition. Longman Scientific & Technical. 696pp.
Dewey, J.F., 1976. Ophiolite obduction. Tectonophysics 31, 93–120. https://doi.org/10.1016/0040-1951(76)90169-4.
Dilek, Y., Flower, M.F.J., 2003. Arc-trench roll-back and forearc accretion: 2. A model template for ophiolites in Albania, Cyprus, and Oman. In: Dilek, Y., Robinson, P.T. (Eds.), Ophiolites in Earth History, 218. Geological Society, London, Special Publication, pp. 43–68. https://doi.org/10.1144/GSL.SP.2003.218.01.04.
Dilek, Y., Furnes, H., 2011. Ophiolite genesis and global tectonics: geochemical and tectonic fingerprinting of ancient oceanic lithosphere. Geol. Soc. Am. Bull. 123, 387–411. https://doi.org/10.1130/B30446.1.
Dubacq, B., Forshaw, J.B., 2024. The composition of metapelitic biotite, white mica and chlorite: a review with implications for solid-solution models. Eur. J. Mineral. 36 (4), 657–685. https://doi.org/10.5194/ejm-36-657-2024.
Dubacq, B., Vidal, O., De Andrade, V., 2010. Dehydration of dioctahedral aluminous phyllosilicates: thermodynamic modelling and implications for thermobarometric estimates. Contrib. Mineral. Petrol. 159 (2), 159–174. https://doi.org/10.1007/s00410-009-0421-6.
Dunning, G.R., Pedersen, R.B., 1988. U/Pb ages of ophiolites and arc-related plutons of the Norwegian Caledonides: implications for the development of Iapetus. Contrib. Mineral. Petrol. 98, 13–23. https://doi.org/10.1007/BF00371904.
Eide, E.A., Lardeaux, J.-M., 2002. A relict blueschist in meta-ophiolite from the central Norwegian Caledonides: discovery and consequences. Lithos 60, 1–19. https://doi.org/10.1016/S0024-4937(01)00074-3.
Elvevold, S., 1988. Petrologiske undersøkelser av kaledonske bergarter i Takvatnområdet, Troms. Unpublished thesis. University of Tromsø, 149 pp.
Faber, C., Stünitz, H., Gasser, D., Jeřábek, P., Kraus, K., Corfu, F., Ravna, E.K., Konopásek, J., 2019. Anticlockwise metamorphic pressure–temperature paths and nappe stacking in the Reisa Nappe complex in the Scandinavian Caledonides, northern Norway: evidence for weakening of lower continental crust before and during continental collision. Solid Earth 10, 117–148. https://doi.org/10.5194/se-10-117-2019.
Fassmer, K., Martinet, I., Miladinova, I., Sprung, P., Froitzheim, N., Fonseca, R.O.C., Münker, C., Janák, M., Kullerud, K., 2020. Lu-Hf geochronology of ultra-high-pressure eclogites from the Tromsø-Nappe, Scandinavian Caledonides: evidence for rapid subduction and exhumation. Int. J. Earth Sci. 109, 1727–1742. https://doi.org/10.1007/s00531-020-01866-0.
Florence, F.P., Spear, F.S., 1991. Effects of diffusional modification of garnet growth zoning on *P-T* path calculations. Contributions to Mineralogy and Petrology 107, 487–500. https://doi.org/10.1007/BF00310683.
Furnes, H., Pedersen, R.B., 1995. Lyngen Magmatic complex: Geology and Geochemistry. Geonytt 22, 30.
Furnes, H., Pedersen, R.B., Stillman, C.J., 1988. The Leka Ophiolite complex, central Norwegian Caledonides: field characteristics and geotectonic significance. J. Geol. Soc. Lond. 145, 401–412. https://doi.org/10.1144/gsjgs.145.3.0401.
Gaidies, F., Heldwein, O.K.A., Yogi, M.T.A.G., Cutts, J.A., Smit, M.A., Rice, A.H.N., 2021. Testing the equilibrium model: an example from the Caledonian Kalak Nappe complex (Finnmark, Arctic Norway). J. Metamorph. Geol. 40 (5), 859–886. https://doi.org/10.1111/jmg.1264.
Gasser, D., Jeřábek, P., Faber, C., Stünitz, H., Menegon, L., Corfu, F., Erambert, M., Whitehouse, M.J., 2015. Behaviour of geochronometers and timing of metamorphic reactions during deformation at lower crustal conditions: phase equilibrium modelling and U-Pb dating of zircon, monazite, rutile and titanite from the Kalak Nappe complex, northern Norway. J. Metamorph. Geol. 33 (5), 513–534. https://doi.org/10.1111/jmg.12131.
Gee, D.G., Stephens, M.B., 2020. Regional context and tectonostratigraphic framework of the early–middle Paleozoic Caledonide orogen, northwestern Sweden. In: Stephens, M.B., Bergman Weihed, J. (Eds.). Geol. Soc. Lond. Mem. 50, 481–494. https://doi.org/10.1144/M50-2017-2.
Gee, D.G., Ladenberger, A., Dahlqvist, P., Majka, J., Be'eri-Shlevin, Y., Frei, D., Thomsen, T., 2014. The Baltoscandian margin detrital zircon signatures of the central Scandes. In: Corfu, F., Gasser, D., Chew, D.M. (Eds.). New perspectives on the Caledonides of Scandinavia and related areas. Geol. Soc. Lond. Spec. Publ. 390, 131–155. https://doi.org/10.1144/SP390.20.
Grenne, T., 1989. Magmatic evolution of the Løkken SSZ Ophiolite, Norwegian Caledonides: relationship between anomalous lavas and high-level intrusions. Geol. J. 24, 251–274. https://doi.org/10.1002/gj.3350240403.
Hayden, L.A., Watson, E.B., Wark, D.A., 2008. A thermobarometer for sphene (titanite). Contrib. Mineral. Petrol. 155, 529–540. https://doi.org/10.1007/s00410-007-0256-y.
Herwegh, M., Mercolli, I., Linckens, J., Müntener, O., 2016. Mechanical anisotropy control- on strain localization in upper mantle shear zones. Tectonics 35, 1177–1204. https://doi.org/10.1002/2015TC004007.
Holland, T., Blundy, J., 1994. Non-ideal interactions in calcic amphiboles and their bearing on amphibole-plagioclase thermometry. Contrib. Mineral. Petrol. 116, 433–447. https://doi.org/10.1007/BF00310910.
Höpfl, S., Konopásek, J., Sláma, J., 2024. Influence of a rigid backstop on the flow pattern during thrusting of the supracrustal Balsfjord Series of the North Norwegian Caledonides. J. Struct. Geol. 182, 105102. https://doi.org/10.1016/j.jsg.2024.105102.
Janák, M., Ravna, E.J.K., Kullerud, K., 2012. Constraining peak P-T conditions in UHP eclogites: calculated phase equilibria in kyanite- and phengite-bearing eclogite of the Tromsø Nappe, Norway. J. Metamorphic Geol. 30 (4), 377–396. https://doi.org/10.1111/j.1525-1314.2011.00971.x.
Janák, M., Borghini, A., Klonowska, I., Yoshida, K., Dujnič, V., Kurylo, S., Froitzheim, N., Petrík, I., Majka, J., 2024. Metamorphism and Partial Melting at UHP Conditions Revealed by Microdiamonds and Melt Inclusions in Metapelitic Gneiss from Heia, Arctic Caledonides, Norway. J. Petrol. 65, 11, egae114. https://doi.org/10.1093/petrology/egae114.
Jessell, M.W., 1986. Grain boundary migration microstructures in a naturally deformed quartzite. J. Struct. Geol. 9, 1007–1014.
Kirkland, C.L., Slagstad, T., Yakymchuk, C., Danišík, M., Rankenburg, K., Kinney, C., Olierook, H., Evans, N.J., 2021. Apatite and biotite thermochronometers help explain an Arctic Caledonide inverted metamorphic gradient. Chem. Geol. 584, 120524. https://doi.org/10.1016/j.chemgeo.2021.120524.
Kohn, M.J., 2017. Titanite Petrochronology. Rev. Mineral. Geochem. 83, 419–441. https://doi.org/10.2138/rmg.2017.83.13.
Kohn, M.J., Spear, F.S., 1990. Two new geobarometers for garnet amphibolites, with applications to southeastern Vermont. Am. Mineral. 75 (1–2), 89–96.
Kowallis, B.J., Christiansen, E.H., Dorais, M.J., Winkel, A., Henze, P., Franzen, L., Mosher, H., 2022. Variation of Fe, Al, and F Substitution in Titanite (Sphene). Geosciences 12 (6), 229. https://doi.org/10.3390/geosciences12060229.
Krogh, E.J., Andresen, A., Bryhni, I., Broks, T.M., Kristensen, S.E., 1990. Eclogites and polyphase P-T cycling in the Caledonian Uppermost Allochthon in Troms, northern Norway. J. Metamorphic Petrol. 8 (3), 289–309. https://doi.org/10.1111/j.1525-1314.1990.tb00474.x.
Kvassnes, A.J.S., Hetland, A., Moen-Eikeland, H., Pedersen, R.B., 2004. The Lyngen Gabbro: the lower crust on an Ordovician Incipient Arc. Contrib. Mineral. Petrol. 148, 358–379. https://doi.org/10.1007/s00410-004-0609-8.
Leake, B.E., Woolley, A.R., Arps, C.E.S., Birch, W.D., Gilbert, M.C., Grice, J.D., Hawthorne, F.C., Kato, A., Kisch, H.J., Krivovichev, V.G., Linthout, K., Laird, J., Mandarino, J.A., Maresch, W.V., Nickel, E.H., Rock, N.M.S., Schumacher, J.C., Smith, D.C., Stephenson, N.C.N., Ungaretti, L., Whittaker, E.J.W., Youzhi, G., 1997. Nomenclature of amphiboles; report of the subcommittee on amphiboles of the International Mineralogical Association, Commission on New Minerals and Mineral Names. Can. Mineral. 35 (1), 219–246.
Lindstrøm, M., Andresen, A., 1992. Early Caledonian high-grade metamorphism within exotic terranes of the Troms Caledonides? Nor. Geol. Tidsskr. 72 (4), 375–379.
Lloyd, G.E., Freeman, B., 1994. Dynamic recrystallisation of quartz and quartzites. J. Struct. Geol. 16, 867–881.
McKerrow, W.S., Mac Niocaill, C., Dewey, J.F., 2000. The Caledonian Orogeny redefined. J. Geol. Soc. Lond. 157 (6), 1149–1154. https://doi.org/10.1144/jgs.157.6.1149.
Menegon, L., Fagereng, Å., 2021. Tectonic pressure gradients during viscous creep drive fluid flow and brittle failure at the base of the seismogenic zone. Geology 49, 1255–1259. https://doi.org/10.1130/G49012.1.
Minsaas, O., Sturt, B.A., 1985. The Ordovician—Silurian clastics sequence overlying the Lyngen Gabbro complex, and its environmental significance. In: Gee, D.G., Sturt, B. A. (Eds.), The Caledonide Orogen –Scandinavia and Related Areas. John Wiley and Sons Ltd., pp. 379–393
Molina, J.F., Moreno, J.A., Castro, A., Rodríguez, C., Fershtater, G.B., 2015. Calcic amphibole thermobarometry in metamorphic and igneous rocks: New calibrations

based on plagioclase/amphibole Al-Si partitioning and amphibole/liquid Mg partitioning. Lithos 232, 286–305. https://doi.org/10.1016/j.lithos.2015.06.027.
Munday, R.J.C., 1974. The geology of the northern half of the Lyngen Peninsula, Troms, Norway. Norsk Geologisk Tidsskrift 54 (1), 49–62.
Nakada, S., 1991. Magmatic processes in titanite-bearing dacites, Central Andes of Chile and Bolivia. Am. Mineral. 76, 548–560.
Olaussen, S., 1976. Paleozoic fossils from Troms, Norway. Nor. Geol. Tidsskr. 56, 457–459.
Oliver, G.J.H., Krogh, T.E., 1995. U-Pb zircon age of 469 ±5 Ma for a metatonalite from the Kjosen Unit of the Lyngen Magmatic complex, northern Norway. Nor. Geol. Unders. 428, 27–32.
Pearce, J.A., 2003. Supra-subduction zone ophiolites: the search for modern analogues. Geol. Soc. Am. Spec. Pap. 373, 269–293. https://doi.org/10.1130/0-8137-2373-6.269.
Pearce, J.A., Lippard, S.J., Roberts, S., 1984. Characteristics and tectonic significance of supra-subduction zone ophiolites. Lond. Geol. Soc. Lond. Spec. Publ. 16, 77–94. https://doi.org/10.1144/GSL.SP.1984.016.01.06.
Randall, B.A.O., 1959. A Preliminary Account of the Geology of the Southern Portion of the Peninsula of Lyngen. University of Dunnam, Troms, North Norway. PhD Thesis, 191 pp.
Ravna, E.J.K., Roux, M.R.M., 2006. Metamorphic Evolution of the Tønsvika Eclogite, Tromsø Nappe−evidence for a New UHPM Province in the Scandinavian Caledonides. Int. Geol. Rev. 48 (10), 861–881. https://doi.org/10.2747/0020-6814.48.10.861.
Ravna, E.J.K., Kullerud, K., Ellingsen, E., 2006. Prograde garnet-bearing ultramafic rocks from the Tromsø Nappe, northern Scandinavian Caledonides. Lithos 92 (3–4), 336–356. https://doi.org/10.1016/j.lithos.2006.03.058.
Reiners, P.W., Brandon, M.T., 2006. Using thermochronology to understand orogenic erosion. Annu. Rev. Earth Planet. Sci. 34, 219–266. https://doi.org/10.1146/annurev.earth.34.031405.125202.
Rice, A.H.N., 1998. Stretching lineations and structural evolution of the Kalak Nappe complex (Middle Allochton) in the Repparfjord-Fægfjord area, Finnmark, northern Norway. Nor. Geol. Tidsskr. 78, 277–289.
Roberts, D., Gee, D.G., 1985. An introduction to the structure of the Scandinavian Caledonides. In: Gee, D.G., Sturt, B.A. (Eds.), The Caledonide Orogen—Scandinavia and Related Areas. John Wiley & Sons, Chichester, pp. 55–68.
Roberts, R.J., Corfu, F., Torsvik, T.H., Ashwal, L.D., Ramsay, D.M., 2006. Short-lived mafic magmatism at 560-570 Ma in the northern Norwegian Caledonides: U-Pb zircon ages from the Seiland Igneous Province. Geol. Mag. 143 (6), 887–903. https://doi.org/10.1017/S0016756806002512.
Roberts, D., Nordgulen, Ø., Melezhik, V., 2007. The Uppermost Allochthon in the Scandinavian Caledonides: From a Laurentian ancestry through Taconian orogeny to Scandian crustal growth on Baltica. In: Hatcher, R.D., Carlson, M.P., McBride, J.H., Martínez Catalán, J.R. (Eds.), 4-D Framework of Continental Crust. Geological Society of America. https://doi.org/10.1130/2007.1200(18).
Rubatto, D., Angiboust, S., 2015. Oxygen isotope record of oceanic and high-pressure metasomatism: a P-T-time-fluid path for the Monviso eclogites (Italy). Contrib. Mineral. Petrol. 170, 44. https://doi.org/10.1007/s00410-015-1198-4.
Schiffer, W.J., 2017. Structural and Metamorphic Implications of the Final Emplacement of the Lyngen Nappe. The Arctic University of Norway, Master Thesis, 107pp.
Searle, M., Cox, J., 1999. Tectonic setting, origin and obduction of the Oman ophiolite. Geol. Soc. Am. Bull., 111(1), 104—122. doi:https://doi.org/10.1130/0016-7606(1999)111%3C0104:TSOAOO%3E2.3.CO;2.
Selbekk, R.S., Furnes, H., Pedersen, R.B., Skjerlie, K., 1998. Contrasting tonalite genesis in the Lyngen Magmatic complex, North Norwegian Caledonides. Lithos 42, 243–268. https://doi.org/10.1016/S0024-4937(97)00045-5.
Selbekk, R.S., Skjerlie, K.P., Pedersen, R.B., 2000. Generation of anorthositic magma by H2 O-fluxed anatexis of silica-undersaturated gabbro: an example from the north Norwegian Caledonides. Geol. Mag. 137 (6), 609–621.
Selbekk, R.S., Bray, C.J., Spooner, E.T.C., 2002. Formation of tonalite in island arcs by seawater-induced anatexis of mafic rocks; evidence from the Lyngen Magmatic complex, North Norwegian Caledonides. Chem. Geol. 182, 69–84. https://doi.org/10.1016/S0009-2541(01)00284-4.
Slagstad, D., 1995a. Rypdalen skjærsone, en oseansk skjærsone i Lyngen magmatiske kompleks. Master thesis. Universitetet i Bergen, 264pp.
Slagstad, D., 1995b. Lyngen Magmatic Complex: Rypdalen Shear Zone; Magmatic and Structural Evolution. Abstract for Norsk Geologisk Forenings XIV Landsmøte, Trondheim.
Slagstad, T., Kirkland, C.L., 2017. The use of detrital zircon data in terrane analysis: A nonunique answer to provenance and tectonostratigraphic position in the Scandinavian Caledonides. Lithosphere 9 (6), 1002–1011. https://doi.org/10.1130/L663.1.
Slagstad, T., Pin, C., Roberts, D., Kirkland, C.L., Grenne, T., Dunning, G., Sauer, S., Andersen, T., 2014. Tectonomagmatic evolution of the early Ordovician suprasubduction-zone ophiolites of the Trondheim Region, Mid-Norwegian Caledonides. Geol. Soc. Lond. Spec. Publ. 390, 541–560. https://doi.org/10.1144/SP390.11.
Slagstad, T., Anderson, M., Saalmann, K., Hagen-Peter, G., 2020. The >494 Ma Lillevik ophiolite fragment (Gratangseidet Igneous complex) near Narvik, Scandinavian Caledonides. Nor. J. Geol. 100, 202022. https://doi.org/10.17850/njg100-4-5.
Soret, M., Larson, K.P., Cottle, J.M., Smit, M., Johnson, A., Shrestha, S., Ali, A., Faisal, S., 2019. Mesozoic to Cenozoic tectono-metamorphic history of the South Pamir–Hindu Kush (Chitral, NW Pakistan): Insights from phase equilibria modelling, and garnet–monazite petrochronology. J. Metamorph. Geol. 37 (5), 633–666. https://doi.org/10.1111/jmg.12479.
Soret, M., Bonnet, G., Agard, P., Larson, K.P., Cottle, J.M., Dubacq, B., Kylander-Clark, A. R.C., Button, M., Rividi, N., 2022. Timescales of subduction initiation and evolution of subduction thermal regimes. Earth Planet. Sci. Lett. 584, 117521. https://doi.org/10.1016/j.epsl.2022.117521.
Stipp, M., Stünitz, H., Heilbronner, R., Schmid, S.M., 2002. The eastern Tonale fault zone: a "natural laboratory" for crystal plastic deformation of quartz over a temperature range from 250 to 700°C. J. Struct. Geol. 24, 1861–1884.
Torsvik, T.H., Smethurst, M.A., Meert, J.G., Van der Voo, R., Mckerrow, W.S., Brasier, M. D., Sturt, B.A., Walderhaug, H.J., 1996. Continental break-up and collision in the Neoproterozoic and Palaeozoic: a tale of Baltica and Laurentia. Earth Sci. Rev. 40, 229–258. https://doi.org/10.1016/0012-8252(96)00008-6.
Vidal, O., De Andrade, V., Lewin, E., Munoz, M., Parra, T., Pascarelli, S., 2006. P-T-deformation-Fe3+/Fe2+ mapping at the thin section scale and comparison with XANES mapping: application to a garnet-bearing metapelite from the Sambagawa metamorphic belt (Japan). J. Metamorph. Geol. 24 (7), 669–683. https://doi.org/10.1111/j.1525-1314.2006.00661.x.
Wakabayashi, J., Dilek, Y., 2003. What constitutes "emplacement" of an ophiolite?: Mechanisms and relationship to subduction initiation and formation of metamorphic soles. In: Dilek, Y., Robinson, P.T. (Eds.). Ophiolites in Earth history. Geol. Soc. Lond. Spec. Publ. 218, 427–448. https://doi.org/10.1144/GSL.SP.2003.218.01.22.
Whitney, D.L., Evans, B.W., 2010. Abbreviations for names of rock-forming minerals. Am. Mineral. 95 (1), 185–187. https://doi.org/10.2138/am.2010.3371.
Wilson, J.T., 1965. A new class of faults and their bearing on continental drift. Nature 207, 343–347. https://doi.org/10.1038/207343a0.
Yogi, M.T.A.G., Gaidies, F., Heldwein, O.K.A., Rice, A.H.N.R., 2024. Mechanisms and durations of metamorphic garnet crystallization in the lower nappes of the Caledonian Kalak Nappe complex, Arctic Norway. J. Metamorphic Petrol. 42 (5), 637–664. https://doi.org/10.1111/jmg.12766.
Zane, A., Sassi, R., Guidotti, C.V., 1998. New data on metamorphic chlorite as a petrogenetic indicator mineral, with special regard to greenschist-facies rocks. Can. Mineral. 36, 713—726.F.
Ziemniak, G., Kośmińska, K., Petrík, I., Janák, M., Walczak, K., Manecki, M., Majka, J., 2019. Th−U−total Pb monazite geochronology records Ordovician (444 Ma) metamorphism/partial melting and Silurian (419 Ma) thrusting in the Kåfjord Nappe, Norwegian Arctic Caledonides. Geol. Carpath. 70 (6), 494–511. https://doi.org/10.2478/geoca-2019-0029.
Zwaan, K.B., Fareth, E., Grogan, P.W., 1998. Geologisk kart over Norge, berggrunnskart TROMSØ, M 1:250.000. Norges geologiske undersøkelse.